Article

Pulse Dipolar ESR of Doubly Labeled Mini TAR DNA and Its Annealing to Mini TAR RNA

Yan Sun,[1] Peter P. Borbat,[2] Vladimir M. Grigoryants,[1] William K. Myers,[1] Jack H. Freed,[2] and Charles P. Scholes[1,*]

[1]Department of Chemistry, University at Albany, State University of New York, Albany, New York; and [2]Department of Chemistry and Chemical Biology and ACERT, Cornell University, Ithaca, New York

ABSTRACT Pulse dipolar electron-spin resonance in the form of double electron electron resonance was applied to strategically placed, site-specifically attached pairs of nitroxide spin labels to monitor changes in the mini TAR DNA stem-loop structure brought on by the HIV-1 nucleocapsid protein NCp7. The biophysical structural evidence was at Ångstrom-level resolution under solution conditions not amenable to crystallography or NMR. In the absence of complementary TAR RNA, double labels located in both the upper and the lower stem of mini TAR DNA showed in the presence of NCp7 a broadened distance distribution between the points of attachment, and there was evidence for several conformers. Next, when equimolar amounts of mini TAR DNA and complementary mini TAR RNA were present, NCp7 enhanced the annealing of their stem-loop structures to form duplex DNA-RNA. When duplex TAR DNA-TAR RNA formed, double labels initially located 27.5 Å apart at the 3′- and 5′-termini of the 27-base mini TAR DNA relocated to opposite ends of a 27 bp RNA-DNA duplex with 76.5 Å between labels, a distance which was consistent with the distance between the two labels in a thermally annealed 27-bp TAR DNA-TAR RNA duplex. Different sets of double labels initially located 26–27 Å apart in the mini TAR DNA upper stem, appropriately altered their interlabel distance to ~35 Å when a 27 bp TAR DNA-TAR RNA duplex formed, where the formation was caused either through NCp7-induced annealing or by thermal annealing. In summary, clear structural evidence was obtained for the fraying and destabilization brought on by NCp7 in its biochemical function as an annealing agent and for the detailed structural change from stem-loop to duplex RNA-DNA when complementary RNA was present.

INTRODUCTION

This structural study uses pulse dipolar spectroscopy (PDS) implemented at the current state of the art (1–3) to understand the change in physical structure of a stem-loop oligonucleotide from HIV-1. The stem-loop structure is found in the TAR (transactivation response) region of TAR DNA and TAR RNA. The binding of NCp7 inhibits self-priming within such a stem-loop, destabilizes stem-loops, and effectively catalyzes the annealing of complementary oligonucleotide strands so that duplexes form between complementary DNA and RNA. This annealing behavior in the presence NCp7 has been shown by gel techniques to occur both in vivo (4) and in vitro (5,6). The purpose of this work is to determine the nature of the oligonucleotide structural change brought on by NCp7 upon mini TAR DNA and then in conjunction with the complementary mini TAR RNA. The functional biochemical relevance of the annealing and the oligonucleotide structural change is that it aids in rapid HIV genome replication and integration into the host.

The in vitro annealing studies were carried out using the 1–55 form of NCp7, which we also use, that has a basic 1–11 tail (5,6). The mini TAR constructs, which we used for this structural study and for our previous dynamic study (7), are also very similar to those used for in vitro annealing (5,6). For our present structural study three pairs of nitroxide labeling sites on mini TAR DNA, which are the SLAB, SLCD, and SLEF sites shown in Fig. 1, were selected. Structural changes reported by SLAB, SLCD, and SLEF constructs occurred as these stem-loops were destabilized by NCp7 or reacted with equimolar complementary mini TAR RNA in the presence of NCp7.

Over the last decade PDS has been widely used to determine distances within doubly labeled oligonucleotide molecules in the range of 1.5–8 nm (8–23). Further developments in PDS methods (3) enable even greater distances to be measured. For example, Fig. 7 *b* of (3) shows how long distances are readily obtained for TAR RNA-TAR DNA complexes. Not only the distance, but distance distributions, can be measured by PDS under solution conditions, which do not lend themselves to high resolution NMR or crystallography. Such distributions give insight into naturally occurring, disorder-inducing processes.

Submitted July 17, 2014, and accepted for publication December 3, 2014.

*Correspondence: cps14@albany.edu

William K. Myers's present address is Inorganic Chemistry Laboratory, Centre for Advanced Electron Spin Resonance (CAESR), University of Oxford, South Parks Road, Oxford OX1 3QR, United Kingdom.

Editor: Timothy Lohman.

© 2015 by the Biophysical Society

0006-3495/15/02/0893/10 $2.00

http://dx.doi.org/10.1016/j.bpj.2014.12.028

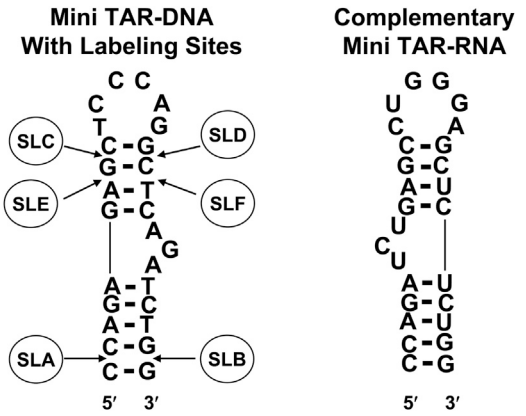

FIGURE 1 The secondary structure of mini TAR DNA together with positions of spin labels attached via phosphorothioate linkages. The complementary mini TAR RNA is also shown. On the mini TAR DNA the spin labels were attached in pairs, SLA-SLB, SLC-SLD, SLE-SLF, and the constructs were called SLAB, SLCD, and SLEF, respectively.

In our previous dynamic study with 9.5 and 236.6 GHz room temperature EPR (electron paramagnetic resonance), single nitroxide labeling sites in the lower stem, loop, and bulge were used to monitor the change in rotational dynamics of mini TAR DNA in the presence of increasing NCp7 concentrations (7). As a function of the ratio of NCp7 to mini TAR DNA, the tumbling time was found to increase with increasing NCp7, implying that more NCp7 was bound as the concentration of NCp7 increased. The tumbling time increased sharply when the ratio of TAR DNA/NCp7 became 1:4, implying the formation of condensates where there were 6–7 TAR bases per NCp7 (7). Evidence for condensates at that coverage of oligonucleotides by NCp7 has previously been reported through application of light scattering techniques (24,25). The condensing function is thought to be important in the annealing process, but the light scattering from condensates is not conducive to fluorescence resonance energy transfer (FRET), and the disorder that results is not conducive to high resolution NMR. The potential for condensing and disorder is, however, not an impediment to PDS. In this work, as a measure of the unwinding and destabilization of the TAR DNA stem structure by NCp7, PDS was used to probe the distance distributions between bilabels at a coverage of ~6–7 bases per NCp7 in the absence of TAR RNA. Because of the small size of the nitroxide probes, their short tethers, and the accurate method for extracting pair distributions (26,27), the pulsed EPR technique provided not only precise interprobe distances (whereas FRET yields estimates of distances if the proper donor-acceptor pair is chosen), but also quantitative data on the distribution of end-to-end distances in NCp7-destabilized mini TAR DNA. We provide, with the power of PDS, clear resolution of explicit distance changes and distance distributions at Ångstrom (i.e., 0.1 nm) resolution and additional structural evidence of multiple conformers.

Distance changes from several pairs of double labels (SLAB, SLCD, SLEF) within mini TAR DNA were next followed in the presence of NCp7 and complementary mini TAR RNA. Where both NCp7 and complementary RNA were present, these measured distances showed marked changes both from the initial stem-loop structures in the absence of NCp7 to the case of duplex DNA-RNA. These distance changes were explicit evidence that NCp7 had catalyzed the annealing of complementary oligonucleotide strands so that duplexes had formed between complementary DNA and RNA. To compare the results of annealing by NCp7, control experiments were also performed on TAR DNA-TAR RNA samples that were thermally annealed in the absence of NCp7. This work thus provides a demonstration of the power of pulse dipolar electron-spin resonance (ESR) for resolving distances and distance distributions of oligonucleotide systems when these systems exhibit multiple conformations.

MATERIALS AND METHODS

Preparation and characterization of spin-labeled mini TAR DNA

Spin labels were attached at the positions SLA, SLB, SLC, SLD, SLE, and SLF of mini TAR DNA (Fig. 1) by the method shown in Fig. 2, using protocols previously described (7). Doubly labeled derivatives at diametrically opposite duplex locations were created as follows: 1) SLAB at the penultimate 3′ and 5′ locations in the lower stem; 2) SLCD in the upper stem near the loop; 3) SLEF in the middle of the upper stem. A thio-methyl-phosphorothioate method of label attachment, indicated in Fig. 2, was used for making SLA, SLB, SLC, SLD, SLE, and SLF (7,14). For SLA and SLB, the thio-amido phosphorothioate method of label attachment was also used for some initial experiments (7). Mini TAR DNA with phosphorothioate modifications was purchased from TriLink (TriLink Bio Technologies, San Diego, CA) or IDT (Integrated DNA Technologies, Skokie, IL). 3-(2-iodoacetamide) proxyl (IPSL) for thio-amido attachment and 3-iodomethyl-(1-oxy-2,2,5,5-tetramethylpyrroline) for thio-methyl attachment were purchased from Toronto Research Chemicals, North York, Ontario, Canada. The detailed preparative protocols for label attachment are provided in the Supporting Material of Sun et al. (7). Purification and characterization of the spin-labeled derivatives were done by high-performance liquid chromatography (HPLC), as shown in Fig. S1 of our Supporting Material. Analytical denaturing gel electrophoresis was used to monitor the formation of the doubly labeled product, as shown in Fig. S2.

Nondenaturing gel-shift annealing assays

These assays were used to probe the annealing process of mini TAR DNA with complementary mini TAR RNA (5,6), where this process is enhanced by increasing NCp7. The primary purpose of these assays was to show the similarity in annealing behavior between unlabeled mini TAR DNA and doubly labeled mini TAR DNA. Separate bands for mini TAR RNA, mini TAR DNA, and the annealed RNA-DNA duplex were observed, where the presence of the latter duplex was greatly enhanced by increasing amounts of NCp7. The bands of unlabeled mini TAR DNA were similar in their location to the bands of the doubly labeled mini TAR DNA. Detailed gel shift annealing assays are presented in Fig. S3. A low intensity annealed mini TAR DNA-mini TAR RNA duplex band appeared even in the absence of NCp7 both for labeled and unlabeled TAR derivatives, consistent with the findings of Vo et al. (6).

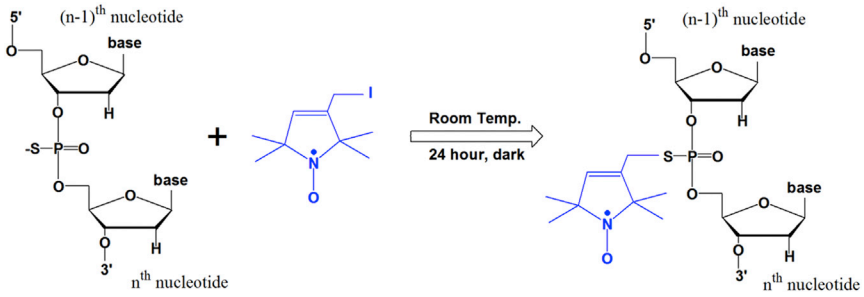

FIGURE 2 The reaction of a phosphorothioate sulfur with 3-iodomethyl-(1-oxy-2,2,5,5-tetramethylpyrroline) in blue to form a phosphorothioate linkage (14).

Thermal melting of doubly labeled mini TAR DNA

The temperature dependence of the UV-260 absorbance was monitored as previously (7) to detect the hyperchromic increase in absorbance at 260 nm associated with the loss of basepairing and thermal melting of the TAR stem-loops. Absorption spectra were obtained by a Cary 3 UV-Vis Spectrophotometer equipped with a thermostated Peltier temperature controller. The controller was ramped at a rate of 0.3°C/min from 20 to 95°C, and the thermal melting profile, as shown below in Fig. 3, was obtained from the first derivative of the absorbance with respect to the temperature. The melting profiles provided melting comparisons of the unlabeled mini TAR DNA with the doubly labeled SLAB, SLCD, and SLEF forms of mini TAR DNA. From these profiles estimates of T_m (melting temperature), ΔH (van't Hoff enthalpy), and ΔS (van't Hoff entropy) were obtained by use of a previously developed nonlinear least-squares fitting routine under the assumption of two-state sequential unfolding (28). The melting profiles of unlabeled mini TAR DNA and the doubly labeled SLAB, SLCD, and SLEF derivatives were acquired under the same buffer conditions, 50 mM HEPES buffer, pH 7.5.

Nucleocapsid protein NCp7

NCp7 was prepared by solid phase peptide synthesis and with analysis methods described previously (29–32). The final NCp7 concentration was determined by using an extinction coefficient of $\varepsilon_{280} = 6050\ M^{-1}\ cm^{-1}$ (33).

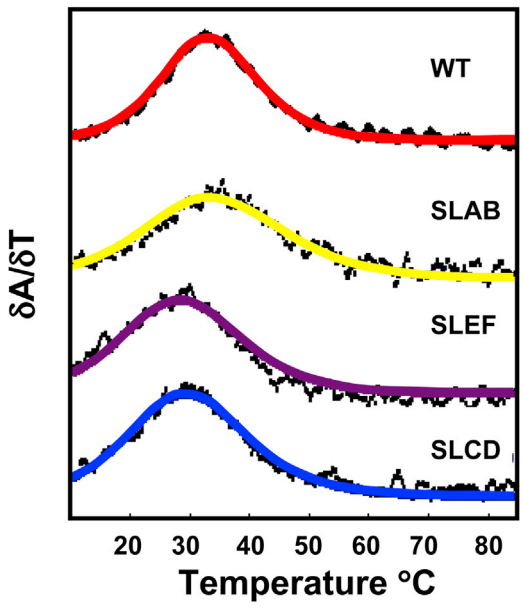

FIGURE 3 This figure provides a comparison of the melting behaviors of unlabeled mini TAR DNA and the SLAB, SLCD, and SLEF doubly labeled derivatives as shown by the first derivative of absorbance at 260 nm.

Pulse dipolar spectroscopy: double electron-electron resonance

DEER measurements were performed in the 50 to 60 K temperature range at a 17.35 GHz working frequency using a home-built Ku-band pulse EPR spectrometer (2,34,35) optimized for double electron-electron resonance (DEER) and double-quantum coherence measurements. The 4-pulse DEER sequence (35–37) was applied with respective $\pi/2$-π-π detection pulse widths of 16 ns, 32 ns, and 32 ns, and a 32 ns π pump pulse was used (7,38). The detection pulses were positioned at the low-field edge of the nitroxide spin-label spectrum and the pump pulse was positioned at the center of the spectrum, so that the frequency separation between detected and pumped pulses was 70 MHz. Interlabel distances were measured in the range of 2–10 nm (20–100 Å) well suited for the DEER, and the DEER evolution time period (τ_2) of 2.5–20 μs was chosen to provide at least two periods of dipolar oscillations for the largest distances encountered in this work. The homogeneous background was removed from the raw time-domain DEER signal, $V(t)$, in a standard way (36,37) by fitting its latter (typically 50%) points of $\log[V(t)]$ to a first or second degree polynomial, extrapolating to early points, and subtracting out. The remainder was then normalized as $(V(t) - 1)/V(0)$ to give the intramolecular dipole-dipole interaction-induced modulation of the time-domain signal. The distances were reconstructed from such baseline corrected and normalized signals (termed dipolar signals in the following) by using the Tikhonov regularization (L-curve) method (27) and refined by the maximum entropy method (26). The distance probability distributions, P(r), in units of nm^{-1}, are thus model free, and not assumed to have a certain profile (e.g., to be Gaussian). Examples of the detailed procedure of DEER signal processing and distance reconstruction are given in Figs. S4–S6 and in Georgieva et al. (38).

Samples of doubly labeled oligonucleotide were typically frozen in 10% glycerol with an oligonucleotide concentration of 50–100 μM. For better resolution of longer distances out to ~100 Å, deuterated solvent was preferable because proton spin-spin interactions diminish the phase memory time for the transient EPR signal and hinder resolution of long-period oscillations and distances beyond ~50 Å. Water that was 98% deuterated and glycerol-d_8 that was 99% perdeuterated were used to prepare deuterated samples. Samples that contained mixtures of double-labeled mini TAR DNA, mini TAR RNA, and NCp7 were allowed to react at room temperature for 5 min before freezing.

Prediction of interlabel distances and distance distributions by the algorithm NASNOX

To independently estimate some distances experimentally measured by DEER, we applied the NASNOX conformational search algorithm, which was developed by Qin and co-workers (11–13,23). Using labels

site-specifically attached in silico to known oligonucleotide Protein Data Bank (PDB) structures, NASNOX introduces a systematic series of spin label rotamer conformations, eliminates those that clash with nearby oligonucleotide moieties, and from the allowed ensemble of rotamers computes inter-NO double-label distances, uncertainty in the distances, and interlabel distance histogram distributions.

RESULTS

Thermal melting of doubly labeled mini TAR DNA

Thermal melting profiles, obtained as the first derivative of the UV-260 absorbance with respect to temperature in the 20–95°C range, are shown in Fig. 3 to provide a melting comparison of the unlabeled and the doubly labeled SLAB, SLCD, and SLEF forms of mini TAR DNA. As described in the Materials and Methods section, values of T_m, ΔH, and ΔS were estimated, and their values are tabulated in Table 1. The melting temperature for unlabeled mini TAR DNA in low salt concentration was lowered by ~3.5°C for SLCD and ~4.5°C for SLED and slightly increased by ~1°C for SLAB. The enthalpy of melting was 37 kcal/mol for unlabeled mini TAR DNA, and this number was diminished by 11, 8, and 8 kcal/mol for SLAB, SLCD, and SLED, respectively. At 20°C the $\Delta G_{20\,^\circ C}$ values ($\Delta G_{20\,^\circ C} = \Delta H - 293\Delta S$), which are the overall free energies of melting at 20°C, were estimated. The values of $\Delta G_{20\,^\circ C}$ indicated that in their stem-loop forms unlabeled mini TAR DNA, SLAB, SLCD, and SLEF, were respectively stabilized by 2.7, 2.0, 1.9, and 1.8 kcal/mol with respect to their melted forms.

Destabilizing doubly labeled mini TAR DNA in the presence of NCp7

SLAB, labeled at the 5′ (SLA) and 3′ (SLB) positions shown in Fig. 1, previously was reported by DEER measurement to be partially unfolded at a molar ratio of 1 mini TAR DNA/4 NCp7 (7). Such unfolding and destabilization were interpreted as part of the NCp7-induced annealing process. In this work SLCD mini TAR DNA with double labels in the upper stem showed evidence for partial unfolding in the presence of a fourfold excess of NCp7, which corresponded to 6–7 TAR bases per NCp7. This partial unfolding, shown by broadening of the initial feature occurring near 26 Å and the appearance of new features in the 30–50 Å range, is indicated in Fig. 4. The pulse dipolar time domain traces

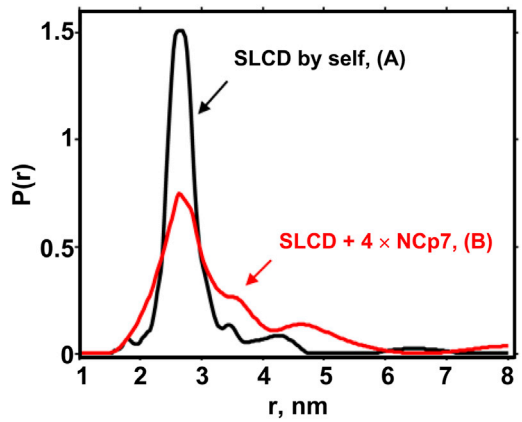

FIGURE 4 This figure provides evidence for the destabilization of the upper stem of doubly labeled SLCD mini TAR DNA. (*A*) Black shows the DEER-derived interprobe SLC-SLD distance distribution, P(r), in units of nm^{-1}, from SLCD mini TAR DNA in the absence of NCp7. (*B*) Red provides the interprobe SLC-SLD distance distribution in the presence of a 1:4 ratio of the SLCD mini TAR DNA construct/NCp7. Sample conditions: 20 mM HEPES, 20 mM NaCl, 0.2 mM $MgCl_2$, pH 7.5. Samples were frozen in 10% glycerol to prevent tube breakage.

relevant to SLCD by itself and with a fourfold excess of NCp7 in Fig. 4 are shown as Fig. S4.

Annealing doubly labeled mini TAR DNA in the presence of complementary mini TAR RNA and NCp7

The annealing process in the presence of complementary mini TAR RNA was monitored to provide evidence for conversion of the destabilized mini TAR DNA to duplex mini TAR DNA-mini TAR RNA. In Fig. 5 we provide the interprobe distance distributions from DEER measurements on the doubly labeled SLAB mini TAR DNA. The interprobe distance distribution of SLAB TAR DNA was unchanged in the presence of an equimolar concentration of TAR RNA. The implication is that little formation (<5%) of duplex TAR DNA-TAR RNA occurred without NCp7 present. For SLAB with no NCp7 present, the separation of labels at the peak of the distribution was 27.5 ± 0.5 Å, and the peak width at half height was 7.0 ± 0.5 Å. The 1:1:4 mixture of the SLAB mini TAR DNA/unlabeled mini TAR RNA/NCp7 provided striking evidence, shown in the red trace of Fig. 5, for a much longer interlabel SLA-SLB distance, consistent with duplex formation. For the red trace

TABLE 1 Melting temperatures, T_m, and the thermodynamic melting parameters ΔH, ΔS, $\Delta G_{20^\circ C}$ for unlabeled mini TAR DNA and doubly labeled SLAB, SLCD, and SLEF constructs

DNA		UNLABELED	SLAB	SLCD	SLEF
Buffer 50 mM Hepes, pH 7.5	T_m (°C)	43.4 ± 1.4	44.4 ± 4.2	39.9 ± 1.8	38.9 ± 2.9
	ΔH (Kcal/mol)	37.0 ± 3.0	25.8 ± 3.4	29.4 ± 3.8	28.9 ± 3.8
	ΔS (cal/mol/K)	117 ± 9	81 ± 11	94 ± 12	93 ± 12
	$\Delta G_{20^\circ C}$ (Kcal/mol)	2.7 ± 0.3	2.0 ± 0.4	1.9 ± 0.3	1.8 ± 0.3
	ΔT_m (°C)	–	+1.0 ± 4.4	−3.5 ± 2.2	−4.5 ± 3.2
	$\Delta\Delta G_{20^\circ C}$ (Kcal/mol)	–	0.7 ± 0.5	0.8 ± 0.4	0.9 ± 0.4

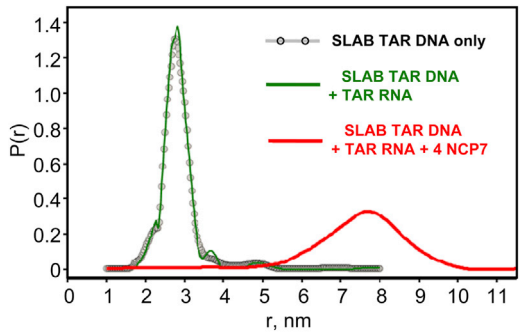

FIGURE 5 DEER distance distributions for doubly labeled mini TAR DNA showing the annealing function of NCp7 when complementary mini TAR RNA was present. The black line is SLAB by itself, the green trace is from a 1:1 mixture of SLAB + mini TAR RNA, and the red trace is a 1:1:4 mixture of SLAB mini TAR DNA/mini TAR RNA/NCp7. Sample conditions were 20 mM HEPES, 20 mM NaCl, 0.2 mM $MgCl_2$, pH 7.5 with 10% glycerol. The samples were deuterated as described in Materials and Methods.

in Fig. 5, the separation of SLA and SLB labels at the peak of the distribution was 76.5 ± 2.0 Å, and the peak width of the interprobe distance distribution was 19.5 ± 2.0 Å. Fig. 5 was obtained with the deuterated solvent system that provides a longer phase memory time for better resolution of distance distributions beyond 60 Å. The pulse dipolar time domain traces relevant to SLAB in Fig. 5 are shown as Fig. S5. We provide in Fig. S7, evidence of the similarity of DEER distance distributions from a NCp7-annealed and from a thermally annealed 1:1 mixture of SLAB mini TAR DNA and mini TAR RNA. (These annealed distributions in Fig. S7 were the result of early measurements, where deuteration was not in use, where the peak positions and the peak widths beyond 60 Å were less accurate, and where double labeling was done with the iodoacetamido spin label that has a longer, flexible tether.)

DEER was next used to follow interlabel distance changes between positions in the upper stem. The double-label positions were at SLC and SLD just below the upper loop, with interlabel distributions shown in Fig. 6 *a*, and SLE and SLF one basepair below C and D, with interlabel distributions shown in Fig. 6 *b*. For these doubly labeled constructs a compendium of traces is presented to show the evolution of the interlabel distance distribution, P(r), due to progressive duplex formation. The duplex formation proceeded in the following order: 1) the initial doubly labeled mini TAR DNA by itself; 2) a 1:1 mixture of doubly labeled mini TAR DNA and unlabeled mini TAR RNA; 3) a 1:1:1 mixture of doubly labeled mini TAR DNA/unlabeled mini TAR RNA/NCp7; 4) a 1:1:4 mixture of doubly labeled mini TAR DNA/mini TAR RNA/NCp7; and 5) a 1:1 mixture of doubly labeled mini TAR DNA/unlabeled mini TAR RNA that had been thermally annealed at 80°C in the absence of NCp7 and then allowed to cool in air to room temperature before freezing. When either SLCD or SLEF were present with equimolar mini TAR RNA, there was a

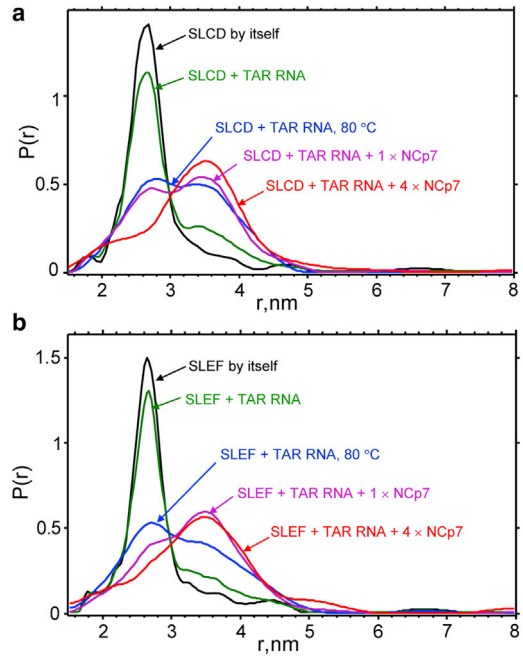

FIGURE 6 The DEER-derived interprobe distance distributions for mini TAR DNA doubly labeled at diametrically opposite phosphorothioate positions CD or EF in the TAR upper stem. The DNA was annealed to complementary unlabeled mini TAR RNA in the presence of NCp7 to form hybrid DNA-RNA duplexes. In panel *a*, the black line is SLCD by itself, the green trace is from a 1:1 mixture of SLCD + mini TAR RNA, the magenta trace is a 1:1:1 mixture of SLCD mini TAR DNA/mini TAR RNA/NCp7, the red trace is from a 1:1:4 mixture of SLCD mini TAR DNA/mini TAR RNA/NCp7, and finally, the blue traces is a thermally annealed mixture of 1:1 mixture of doubly labeled SLCD and mini TAR RNA. Panel *b* shows the same combinations as panel *a*, but with SLEF substituted for SLCD. Sample conditions were 20 mM HEPES, 20 mM NaCl, 0.2 mM MgCl2, pH 7.5 with 10% glycerol. The samples were deuterated as described in Materials and Methods.

slight increase in a species having a larger interlabel distance of ~35 Å, implying that a small amount of annealing was occurring in the absence of NCp7. The presence of NCp7 catalyzed duplex DNA-RNA formation shown by the feature with the interlabel 35 Å distance. The pulse dipolar time domain traces relevant to SLCD and SLEF in Fig. 6 are shown as Fig. S6.

The separation of double labels for both SLCD by itself in Fig. 6 *a* and SLEF by itself in Fig. 6 *b* was 26–27 Å and the separation of labels increased to ~35 Å when the doubly labeled mini TAR DNA was annealed with complementary mini TAR RNA. Distances between labels within SLAB, SLCD, or SLEF in duplex mini TAR RNA-DNA are shown schematically in Fig. 7, and the details of interlabel distances and the interlabel distribution widths are provided in Table 2. Although the distributions showing conversion from stem-loop to apparent duplex superficially seem to show an isosbestic point near 30 Å, there appear to be more species, especially in the presence of fourfold excess NCp7, than just the original stem-loop with the peak near 27 Å and the RNA-DNA duplex with the peak near 35 Å.

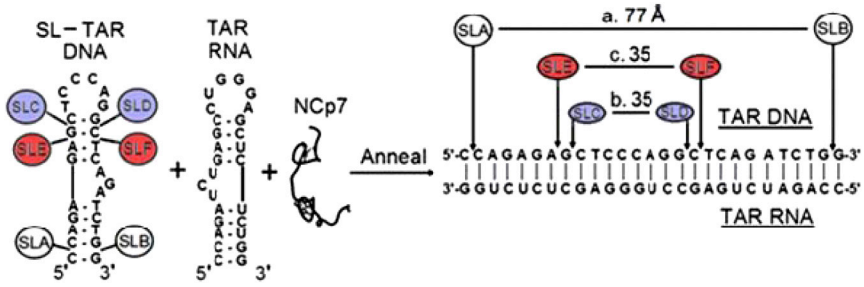

FIGURE 7 Summary of most probable interspin label distances from DEER measurements for the annealed TAR DNA-TAR RNA species of three different samples SLAB, SLCD, and SLEF.

There is a broad shoulder with amplitude extending above 50 Å, in particular for SLED in 1:1:4 DNA/RNA/NCp7, implying the presence of other possibly more disordered species. The presence of these species may diminish the amount of available doubly labeled TAR DNA for duplex formation.

Predicted inter-NO distances compared to DEER findings

The NASNOX routine was developed (13,14) to estimate interlabel distances between double labels attached via phosphorothioate linkages. NASNOX is an efficient conformational search algorithm to accurately predict the internitroxide distances and distributions from rotamer ensembles of phosphorothioate-attached spin labels; the predictions are obtained within minutes on a PC, without the substantial computational resources required for molecular dynamics computations (13,14). Application of NASNOX requires that spin labels be attached in silico to known oligonucleotide PDB model structures, which are not themselves varied during the application of the NASNOX algorithm. For estimating distances between the labels SLA and SLB, SLC and SLD, or SLE and SLF when they were attached diametrically opposite one another in duplex regions of the TAR DNA stem-loop, a duplex DNA structure (PDB 1CS2 (11,39)) was initially chosen. Labels were then attached in silico to this structure and interlabel distances, distribution widths, and interlabel distance histograms were computed. For DNA-RNA hybrid duplexes, relevant to the DNA-RNA duplexes in which SLC and SLD or SLE and SLF reside after annealing, a duplex DNA-RNA model structure (PDB 1EFS (40)) was chosen and labels then attached to it in silico. Detailed NASNOX results are tabulated (Table S1) and compared to DEER results. Interlabel histograms for SLCD and SLEF are compared to DEER spectra in Figs. S8 and S9. The distances and distance distributions obtained from NASNOX were in excellent agreement with those obtained by DEER.

In the TAR DNA-TAR RNA 27 bp duplex, SLA and SLB were separated by 25 phosphates, as indicated in Fig. 7. PDB structures of such lengthy duplex forms are not available, and NASNOX, which requires preexisting PDB structures, is therefore not immediately useful. To approximate the distance between phosphorothioate-attached SLA and SLB spin labels near the opposite ends of a 27-mer DNA-RNA duplex, we worked from literature estimates of the axial rise and the angular rotation per residue (41,42). The calculation of the interlabel distance is explained in the Supporting Material and given in Table S1. For a 25 phosphate separation, the prediction was for a SLA-SLB separation of 74.5 ± 2.8 Å, in excellent agreement with the separation of 76.5 ± 2.0 Å obtained by DEER.

TABLE 2 Interlabel distances and distribution widths of doubly labeled mini TAR DNA

Sample	⟨rDEER⟩ (Å)[a]	$W_{1/2}$ (Å)[a]
SLAB by itself	27.5 ± 0.5	7.0 ± 0.5
SLCD by itself	26.8 ± 0.4	5.2 ± 0.4
SLEF by itself	26.3 ± 0.4	4.3 ± 0.4
1:1:4 SLCD/mini TAR RNA/NCp7	35.1 ± 0.6	10.8 ± 1.0
1:1:4 SLEF/mini TAR RNA/NCp7[b]	34.8 ± 0.6	14.0 ± 1.0
1:1:4 SLAB/mini TAR RNA/NCp7	76.5 ± 2.0	19.5 ± 2.0

[a]⟨rDEER⟩ and $W_{1/2}$ are the respective experimental interlabel distance and the full peak width at half height of the interlabel distance distribution, as determined experimentally by DEER.

[b]In the presence of a fourfold excess of NCp7 with respect to mini TAR DNA and mini TAR RNA, there is evidence for a broad shoulder in the interlabel distribution that extends above 50 Å separation; it is most notable in the SLEF sample.

DISCUSSION

Structural and thermodynamic differences between the SLAB, SLCD, and SLEF spin-labeled constructs

The thermal melting temperatures of SLAB, SLCD, and SLEF constructs were within 1.5% (in °K) of native mini TAR DNA. However, the enthalpies (ΔH) and entropies (ΔS) of melting for doubly labeled SLAB, SLCD, and SLEF were smaller by ~25% than those of native mini TAR DNA, reflecting the perturbation to lower and upper stem formation from phosphorothioate label attachment. If the entropy of all melted forms is about the same, then the smaller value of ΔS for SLAB (81 cal/mol/K), compared to ΔS for SLCD and SLEF (93–94 cal/mol/K), implies the greater disorder of SLAB in its folded form. The SLA and SLB labels are immediately adjacent to the 3′–5′ termini

of the lower duplex region, a region which has exhibited evidence by NMR (43) and FRET (44–46) for intrinsic destabilization even before spin labeling. The peak widths (full width at half height) of the interlabel distributions diminished in the order SLAB, SLCD, SLEF from 7.0 to 5.2 to 4.3 Å. The broader interprobe distance distribution of SLAB, compared to SLCD and SLEF, is consistent by its implication of disorder with the greater entropic destabilization in the lower stem. In conclusion, the DEER technique provided a comparison of the disorder in separate oligonucleotide domains.

In the absence of NCp7 and complementary RNA, the doubly labeled SLAB showed an interlabel distance of 27.5 Å (Fig. 5), whereas SLCD and SLEF mini TAR DNA constructs (Fig. 6, *a* and *b*), both showed slightly smaller interlabel distances of 26.8 and 26.3 Å, respectively. All of these interlabel distances are similar to each other and within an 1.5 Å of NASNOX predictions (Table S1). NASNOX was used with the starting point of an intact duplex DNA structure, which is not varied throughout the NASNOX algorithm (13,14). If the interlabel distances between diametrically opposite labels in stem regions had markedly differed from NASNOX predictions and from each other, the strong implication would have been for a marked perturbation to the duplex stem-loop structure due to the spin labels. There was no such structural perturbation.

NCp7-mediated destabilization of doubly labeled mini TAR DNA

In the ambient temperature 9.5 GHz ESR work of Sun et al. (7), done at a ratio of 1 mini TAR 27-mer per 4 NCp7 (i.e., ~6–7 TAR bases per NCp7), the tumbling times of the spin labels in stem, loop, and bulge of mini TAR DNA markedly increased from ~1 ns to times longer than ~5 ns. This was attributed to the formation of an NCp7-mini TAR DNA condensate, naturally favored at the 1:4 ratio by the 1–55 NCp7 (55-mer) with its highly basic 1–11 tail. At this ratio of NCp7 coverage significant annealing was known to occur (6). This 1:4 ratio of mini TAR DNA to NCp7 was chosen here to probe the biophysical structural implications of annealing under condensing conditions which are not amenable to NMR or FRET.

DEER evidence for NCp7-induced fraying and disorder of the doubly labeled SLAB was previously reported in the lower stem; see Fig. 8 *C* of Sun et al. (7). In this work, DEER spectroscopy of doubly labeled SLCD mini TAR DNA with a 1:4 mini TAR DNA to NCp7 coverage and no TAR RNA present showed that the upper stem also became frayed and disordered (Fig. 4). Although as found in unperturbed SLCD there was a substantial peak at 27 Å in the interlabel distribution, this distribution was considerably broader in the presence of fourfold NCp7. There were also conformers having longer interprobe distances of ~35 Å and 45 Å. The previously studied SLAB was in an intrinsically more unstable region than the upper stem where SLCD is located. There were relatively more conformers with interprobe distances >35 Å for SLAB than for SLCD.

This DEER study notably showed that the upper stem can also be destabilized by NCp7. Overall, DEER measurements show the structural nature of destabilization under conditions where annealing happens. The aggregating sample conditions here of 4 NCp7 per 1 mini TAR 27-mer demonstrate how DEER is able to resolve structure and structural distributions that only could be inferred by fluorescence techniques or by FRET. (See detailed discussion and comparison of DEER and FRET findings in the Supporting Material.)

Annealing doubly labeled mini TAR DNA with mini TAR RNA

For SLAB, SLCD, and SLEF, the presence of mini TAR DNA, mini TAR RNA, and NCp7 in a ratio of 1:1:4 led to a duplex RNA-DNA form. The comparison of interlabel distributions for the NCp7-annealed duplex to the distributions for a thermally annealed mini TAR DNA-mini TAR RNA duplex showed at least as complete a conversion by NCp7 annealing as did thermal annealing. One obvious implication of this comparison is that the ~5 min time for allowing mini TAR DNA, mini TAR RNA, and NCp7 to react was sufficient for conversion to the duplex. The biophysical importance is that detailed structural evidence at Ångstrom resolution is provided by DEER for the stem-loop to duplex conversion, and the NCp7-induced conversion to the DNA-RNA duplex is compared to conversion by thermal annealing.

For SLEF and SLCD the presence of mini TAR DNA, mini TAR RNA, and NCp7 in a 1:1:1 ratio was sufficient to convert most of the mini TAR DNA and mini TAR RNA to duplex form. However, a detailed comparison of the interlabel distributions resulting from the 1:1:1 and 1:1:4 ratios showed that the 1:1:1 ratio left more of the original stem-loop unreacted, as shown by retention of a feature at 27 Å. The 1:1:4 ratio also gave rise to a broad feature extending up to ~50 Å that implies the existence of unwound, nonduplex mini TAR DNA and possibly indicated that the duplex form may have been somewhat destabilized at the 1:1:4 ratio.

A number of stem-loop RNA and DNA constructs with specifically bound NCp7 complexes have been characterized by NMR study at a 1:1 oligonucleotide/NCp7 ratio (43,47–49). One additional NCp7 bound to mini TAR DNA beyond the first was inferred by isothermal calorimetry, but not verified by NMR (43), although that study used 11–55 NCp7 lacking the basic 1–10 tail. For binding of basic 1–55 NCp7 elsewhere than to unpaired loop and bulge regions, NCp7 has been proposed to bind nonspecifically (24,47–49). NCp7 may well operate as annealing catalyst under condensing conditions without

the necessity for forming stoichiometric complexes (24). The study of NCp7 binding to model oligonucleotides by numerous spectroscopic techniques and mass spectrometry showed a complicated compendium of species exhibiting multivalency, i.e., 1:1:, 2:1, 2:2, 1:2, and higher order complexes (50). It is not clear at either the 1:1:1 or 1:1:4 DNA/RNA/NCp7 ratio, where NCp7 is an effective catalyst for annealing, that there is or should be a well-ordered stoichiometric complex of NCp7, especially to the final duplex RNA-DNA product. Regardless of the precise mode of action of NCp7, the critical point shown by our DEER study is that NCp7 does indeed convert stem-loops to duplex DNA-RNA having the definitive structural signature expected for a duplex.

CONCLUSIONS

With strategically placed nitroxide double labels, we have obtained evidence via DEER distance measurements for the structural changes due to NCp7-induced fraying of mini TAR DNA and for NCp7-induced annealing of mini TAR DNA with complementary mini TAR RNA. Using double labels within the upper and lower mini TAR DNA stem, DEER provided interprobe distributions that showed NCp7-induced fraying, that is, evidence at Ångstrom resolution for a structural change of the mini TAR DNA itself. DEER showed the large 25 to 80 Å structural change undergone by double labels on the mini TAR DNA as the DNA conformation changed in the presence of complementary mini TAR RNA from a DNA hairpin to DNA in an RNA-DNA duplex. Other techniques provide qualitative insight, e.g., by FRET efficiency changes (discussed in the Supporting Material) or by gel retardation assays. Detail of the structural change is shown more explicitly by quantitative distance measurements using DEER spectroscopy. Even though this study was carried out on just a 27-mer, it points to the emergence of PDS as a major contributor in elucidating larger looped and knotted tertiary structures from biologically relevant oligonucleotide and protein-oligonucleotides complexes. An application of PDS to another RNA-protein system has just been reported (51).

Supporting Material

Protocols are provided for the HPLC purification, the denaturing gel assay, and the gel-shift annealing assay of doubly labeled mini TAR, including, 1) Fig. S1, which shows the HPLC purification trace for doubly labeled mini TAR DNA, Fig. S2, which shows analytical gel traces for doubly labeled mini TAR DNA, and Fig. S3, which shows gel shift annealing assays of mini TAR DNA with complementary mini TAR RNA; 2) Figs. S4–S6, which show the dipolar evolution transients that respectively lead to the interlabel distances for SLCD in Fig. 4, SLAB in Fig. 5, and SLCD and SLEF in Fig. 6; 3) Fig. S7 shows the similarity in SLA-SLB interlabel distances between NCp7-annealed and thermally annealed 1:1 mixtures of doubly labeled mini DNA and mini TAR RNA; 4) details of the application of the NASNOX method and a tabulated comparison of NASNOX findings with DEER findings; 5) Figs. S8 and S9, respectively, provide the comparison of the experimental DEER internitroxide distributions of SLCD (Fig. 6 *a*) and SLEF (Fig. 6 *b*) to internitroxide histograms computed from NASNOX; and 7) a discussion of the complementary nature of PDS and FRET findings.

SUPPORTING MATERIAL

Supporting Materials and Methods, nine figures, and one table are available at http://www.biophysj.org/biophysj/supplemental/S0006-3495(14)04775-4.

ACKNOWLEDGMENTS

We are grateful to Prof. Carla Theimer, Department of Chemistry, University at Albany, for providing lab space and technical advice for the preparation and characterization of oligonucleotides and to Prof. Peng Chen, Department of Chemistry and Chemical Biology, Cornell University, for a helpful discussion on FRET.

This work was supported by the National Institutes of Health (NIH) (GM066253-01A1 and 3RO1GM06625304S1 to C.P.S.), the NIH/National Institute of General Medical Sciences (NIGMS) (grant P41GM103521 to J.H.F.), and a Faculty Research Award Program-Category A grant from the University at Albany to C.P.S.

SUPPORTING CITATIONS

References (52–62) appear in the Supporting Material.

REFERENCES

1. Polyhach, Y., E. Bordignon, …, G. Jeschke. 2012. High sensitivity and versatility of the DEER experiment on nitroxide radical pairs at Q-band frequencies. *Phys. Chem. Chem. Phys.* 14:10762–10773.
2. Borbat, P. P., E. R. Georgieva, and J. H. Freed. 2013. Improved sensitivity for long-distance measurements in biomolecules: five-pulse double electron-electron resonance. *J. Phys. Chem. Lett.* 4:170–175.
3. Borbat, P. P., and J. H. Freed. 2014. Pulse dipolar ESR: distance measurements. *In* Structural Information from Spin-Labels and Intrinsic Paramagnetic Centers in the Biosciences (Structure and Bonding). J. R. Harmer and C. R. Timmel, editors. Springer Heidelberg, Germany; New York, pp. 1–82.
4. Johnson, P. E., R. B. Turner, …, M. F. Summers. 2000. A mechanism for plus-strand transfer enhancement by the HIV-1 nucleocapsid protein during reverse transcription. *Biochemistry.* 39:9084–9091.
5. Vo, M. N., G. Barany, …, K. Musier-Forsyth. 2009. HIV-1 nucleocapsid protein switches the pathway of transactivation response element RNA/DNA annealing from loop-loop “kissing” to “zipper”. *J. Mol. Biol.* 386:789–801.
6. Vo, M. N., G. Barany, …, K. Musier-Forsyth. 2006. Mechanistic studies of mini-TAR RNA/DNA annealing in the absence and presence of HIV-1 nucleocapsid protein. *J. Mol. Biol.* 363:244–261.
7. Sun, Y., Z. Zhang, …, C. P. Scholes. 2012. The internal dynamics of mini c TAR DNA probed by electron paramagnetic resonance of nitroxide spin-labels at the lower stem, the loop, and the bulge. *Biochemistry.* 51:8530–8541.

8. Schiemann, O., A. Weber, …, S. T. Sigurdsson. 2003. Nanometer distance measurements on RNA using PELDOR. *J. Am. Chem. Soc.* 125:3434–3435.
9. Borbat, P. P., J. H. Davis, …, J. H. Freed. 2004. Measurement of large distances in biomolecules using double-quantum filtered refocused electron spin-echoes. *J. Am. Chem. Soc.* 126:7746–7747.
10. Schiemann, O., N. Piton, …, T. F. Prisner. 2004. A PELDOR-based nanometer distance ruler for oligonucleotides. *J. Am. Chem. Soc.* 126:5722–5729.
11. Cai, Q., A. K. Kusnetzow, …, P. Z. Qin. 2006. Site-directed spin labeling measurements of nanometer distances in nucleic acids using a sequence-independent nitroxide probe. *Nucleic Acids Res.* 34:4722–4730.
12. Cai, Q., A. K. Kusnetzow, …, P. Z. Qin. 2007. Nanometer distance measurements in RNA using site-directed spin labeling. *Biophys. J.* 93:2110–2117.
13. Price, E. A., B. T. Sutch, …, I. S. Haworth. 2007. Computation of nitroxide-nitroxide distances in spin-labeled DNA duplexes. *Biopolymers.* 87:40–50.
14. Qin, P. Z., I. S. Haworth, …, H. He. 2007. Measuring nanometer distances in nucleic acids using a sequence-independent nitroxide probe. *Nat. Protoc.* 2:2354–2365.
15. Schiemann, O., and T. F. Prisner. 2007. Long-range distance determinations in biomacromolecules by EPR spectroscopy. *Q. Rev. Biophys.* 40:1–53.
16. Singh, V., M. Azarkh, …, M. Drescher. 2009. Human telomeric quadruplex conformations studied by pulsed EPR. *Angew. Chem. Int. Ed. Engl.* 48:9728–9730.
17. Kim, N. K., M. K. Bowman, and V. J. DeRose. 2010. Precise mapping of RNA tertiary structure via nanometer distance measurements with double electron-electron resonance spectroscopy. *J. Am. Chem. Soc.* 132:8882–8884.
18. Krstić, I., O. Frolow, …, T. F. Prisner. 2010. PELDOR spectroscopy reveals preorganization of the neomycin-responsive riboswitch tertiary structure. *J. Am. Chem. Soc.* 132:1454–1455.
19. Sicoli, G., F. Wachowius, …, C. Höbartner. 2010. Probing secondary structures of spin-labeled RNA by pulsed EPR spectroscopy. *Angew. Chem. Int. Ed. Engl.* 49:6443–6447.
20. Nguyen, P., and P. Z. Qin. 2012. RNA dynamics: perspectives from spin labels. *Wiley Interdiscip. Rev. RNA.* 3:62–72.
21. Romainczyk, O., B. Endeward, …, J. W. Engels. 2011. The RNA-DNA hybrid structure determined by EPR, CD and RNase H1. *Mol. Biosyst.* 7:1050–1052.
22. Wunnicke, D., D. Strohbach, …, H. J. Steinhoff. 2011. Ligand-induced conformational capture of a synthetic tetracycline riboswitch revealed by pulse EPR. *RNA.* 17:182–188.
23. Zhang, X., C. S. Tung, …, P. Z. Qin. 2012. Global structure of a three-way junction in a phi29 packaging RNA dimer determined using site-directed spin labeling. *J. Am. Chem. Soc.* 134:2644–2652.
24. Vo, M. N., G. Barany, …, K. Musier-Forsyth. 2009. Effect of Mg(2+) and Na(+) on the nucleic acid chaperone activity of HIV-1 nucleocapsid protein: implications for reverse transcription. *J. Mol. Biol.* 386:773–788.
25. Paoletti, A. C., M. F. Shubsda, …, P. N. Borer. 2002. Affinities of the nucleocapsid protein for variants of SL3 RNA in HIV-1. *Biochemistry.* 41:15423–15428.
26. Chiang, Y. W., P. P. Borbat, and J. H. Freed. 2005. Maximum entropy: a complement to Tikhonov regularization for determination of pair distance distributions by pulsed ESR. *J. Magn. Reson.* 177:184–196.
27. Chiang, Y. W., P. P. Borbat, and J. H. Freed. 2005. The determination of pair distance distributions by pulsed ESR using Tikhonov regularization. *J. Magn. Reson.* 172:279–295.
28. Theimer, C. A., Y. Wang, …, D. P. Giedroc. 1998. Non-nearest neighbor effects on the thermodynamics of unfolding of a model mRNA pseudoknot. *J. Mol. Biol.* 279:545–564.
29. Zhang, Z., X. Xi, …, C. B. Karim. 2008. Rotational dynamics of HIV-1 nucleocapsid protein NCp7 as probed by a spin label attached by peptide synthesis. *Biopolymers.* 89:1125–1135.
30. Xi, X., Y. Sun, …, C. P. Scholes. 2008. HIV-1 nucleocapsid protein NCp7 and its RNA stem loop 3 partner: rotational dynamics of spin-labeled RNA stem loop 3. *Biochemistry.* 47:10099–10110.
31. Karim, C. B., T. L. Kirby, …, D. D. Thomas. 2004. Phospholamban structural dynamics in lipid bilayers probed by a spin label rigidly coupled to the peptide backbone. *Proc. Natl. Acad. Sci. USA.* 101:14437–14442.
32. Karim, C. B., Z. Zhang, and D. D. Thomas. 2007. Synthesis of TOAC spin-labeled proteins and reconstitution in lipid membranes. *Nat. Protoc.* 2:42–49.
33. Tummino, P. J., J. D. Scholten, …, D. Hupe. 1996. The in vitro ejection of zinc from human immunodeficiency virus (HIV) type 1 nucleocapsid protein by disulfide benzamides with cellular anti-HIV activity. *Proc. Natl. Acad. Sci. USA.* 93:969–973.
34. Borbat, P. P., R. H. Crepeau, and J. H. Freed. 1997. Multifrequency two-dimensional Fourier transform ESR: an X/Ku-band spectrometer. *J. Magn. Reson.* 127:155–167.
35. Borbat, P. P., and J. H. Freed. 2007. Measuring distances by pulsed dipolar ESR spectroscopy: spin-labeled histidine kinases. *Methods Enzymol.* 423:52–116.
36. Pannier, M., S. Veit, …, H. W. Spiess. 2000. Dead-time free measurement of dipole-dipole interactions between electron spins. *J. Magn. Reson.* 142:331–340.
37. Jeschke, G., and Y. Polyhach. 2007. Distance measurements on spin-labelled biomacromolecules by pulsed electron paramagnetic resonance. *Phys. Chem. Chem. Phys.* 9:1895–1910.
38. Georgieva, E. R., A. S. Roy, …, J. H. Freed. 2012. Effect of freezing conditions on distances and their distributions derived from Double Electron Electron Resonance (DEER): a study of doubly-spin-labeled T4 lysozyme. *J. Magn. Reson.* 216:69–77.
39. Leporc, S., O. Mauffret, …, S. Fermandjian. 1999. An NMR and molecular modelling analysis of d(CTACTGCTTTAG). d(CTAAAGCAG TAG) reveals that the particular behaviour of TpA steps is related to edge-to-edge contacts of their base-pairs in the major groove. *Nucleic Acids Res.* 27:4759–4767.
40. Hantz, E., V. Larue, …, T. Huynh Dinh. 2001. Solution conformation of an RNA–DNA hybrid duplex containing a pyrimidine RNA strand and a purine DNA strand. *Int. J. Biol. Macromol.* 28:273–284.
41. Gyi, J. I., A. N. Lane, …, T. Brown. 1998. Solution structures of DNA.RNA hybrids with purine-rich and pyrimidine-rich strands: comparison with the homologous DNA and RNA duplexes. *Biochemistry.* 37:73–80.
42. Saenger, W. 1984. Principles of Nucleic Acid Structure. Springer-Verlag, New York.
43. Bazzi, A., L. Zargarian, …, O. Mauffret. 2011. Structural insights into the cTAR DNA recognition by the HIV-1 nucleocapsid protein: role of sugar deoxyriboses in the binding polarity of NC. *Nucleic Acids Res.* 39:3903–3916.
44. Bernacchi, S., S. Stoylov, …, Y. Mély. 2002. HIV-1 nucleocapsid protein activates transient melting of least stable parts of the secondary structure of TAR and its complementary sequence. *J. Mol. Biol.* 317:385–399.
45. Cosa, G., E. J. Harbron, …, P. F. Barbara. 2004. Secondary structure and secondary structure dynamics of DNA hairpins complexed with HIV-1 NC protein. *Biophys. J.* 87:2759–2767.
46. Zargarian, L., I. Kanevsky, …, O. Mauffret. 2009. Structural and dynamic characterization of the upper part of the HIV-1 cTAR DNA hairpin. *Nucleic Acids Res.* 37:4043–4054.
47. Summers, M. F., L. E. Henderson, …, D. R. Hare. 1992. Nucleocapsid zinc fingers detected in retroviruses: EXAFS studies of intact viruses and the solution-state structure of the nucleocapsid protein from HIV-1. *Protein Sci.* 1:563–574.

48. De Guzman, R. N., Z. R. Wu, …, M. F. Summers. 1998. Structure of the HIV-1 nucleocapsid protein bound to the SL3 psi-RNA recognition element. *Science.* 279:384–388.

49. Amarasinghe, G. K., J. Zhou, …, M. F. Summers. 2001. Stem-loop SL4 of the HIV-1 psi RNA packaging signal exhibits weak affinity for the nucleocapsid protein. structural studies and implications for genome recognition. *J. Mol. Biol.* 314:961–970.

50. Fisher, R. J., M. J. Fivash, …, A. Rein. 2006. Complex interactions of HIV-1 nucleocapsid protein with oligonucleotides. *Nucleic Acids Res.* 34:472–484.

51. Duss, O., M. Yulikov, …, F. H. Allain. 2014. EPR-aided approach for solution structure determination of large RNAs or protein-RNA complexes. *Nat. Commun.* 5:3669.

52. Wang, H., K. Musier-Forsyth, …, P. F. Barbara. 2013. Single-molecule spectroscopic study of dynamic nanoscale DNA bending behavior of HIV-1 nucleocapsid protein. *J. Phys. Chem. B.* 117:4183–4196.

53. Chan, B., K. Weidemaier, …, K. Musier-Forsyth. 1999. Intra-tRNA distance measurements for nucleocapsid protein-dependent tRNA unwinding during priming of HIV reverse transcription. *Proc. Natl. Acad. Sci. USA.* 96:459–464.

54. Hong, M. K., E. J. Harbron, …, K. Musier-Forsyth. 2003. Nucleic acid conformational changes essential for HIV-1 nucleocapsid protein-mediated inhibition of self-priming in minus-strand transfer. *J. Mol. Biol.* 325:1–10.

55. Liu, H. W., G. Cosa, …, P. F. Barbara. 2005. Single-molecule FRET studies of important intermediates in the nucleocapsid-protein-chaperoned minus-strand transfer step in HIV-1 reverse transcription. *Biophys. J.* 89:3470–3479.

56. Liu, H. W., Y. Zeng, …, P. F. Barbara. 2007. Insights on the role of nucleic acid/protein interactions in chaperoned nucleic acid rearrangements of HIV-1 reverse transcription. *Proc. Natl. Acad. Sci. USA.* 104:5261–5267.

57. Zeng, Y., H. W. Liu, …, P. F. Barbara. 2007. Probing nucleation, reverse annealing, and chaperone function along the reaction path of HIV-1 single-strand transfer. *Proc. Natl. Acad. Sci. USA.* 104:12651–12656.

58. Wang, H., Y. S. Yeh, and P. F. Barbara. 2009. HIV-1 nucleocapsid protein bends double-stranded nucleic acids. *J. Am. Chem. Soc.* 131:15534–15543.

59. Beltz, H., E. Piémont, …, Y. Mély. 2004. Role of the structure of the top half of HIV-1 cTAR DNA on the nucleic acid destabilizing activity of the nucleocapsid protein NCp7. *J. Mol. Biol.* 338:711–723.

60. Beltz, H., J. Azoulay, …, Y. Mély. 2003. Impact of the terminal bulges of HIV-1 cTAR DNA on its stability and the destabilizing activity of the nucleocapsid protein NCp7. *J. Mol. Biol.* 328:95–108.

61. Godet, J., and Y. Mély. 2010. Biophysical studies of the nucleic acid chaperone properties of the HIV-1 nucleocapsid protein. *RNA Biol.* 7:687–699.

62. Gopich, I. V., and A. Szabo. 2011. Theory of single-molecule FRET efficiency histograms. *In* Single-Molecule Biophysics. John Wiley & Sons, Hoboken, NJ, pp. 245–297.

Biophysical Journal

Supporting Material

Pulse Dipolar ESR of Doubly Labeled Mini TAR DNA and Its Annealing to Mini TAR RNA

Yan Sun, Peter P. Borbat, Vladimir M. Grigoryants, William K. Myers, Jack H. Freed, and Charles P. Scholes

SUPPORTING MATERIAL

Table of Contents

Protocol for Anion Exchange HPLC Purification of Spin-Labeled mini TAR DNA.

Anion-exchange HPLC was used to remove the excess nitroxide spin label from the reaction mixture and to separate unlabeled and partially labeled mini TAR DNA from doubly-labeled. The reaction mixture was subjected to anion-exchange HPLC using a PA-100 column (4 X 250 mm^2, Dionex Inc., Sunnyville, CA) at a pressure of approximately 2000 psi. (For later work a Biorad FPLC unit, which would produce 1200 psi, was employed.) Nucleic acids were eluted using a low salt stationary phase (buffer A: 1 mM $NaClO_4$, 20mM Tris–HCl, pH 6.8 and 20% v/v acetonitrile) and a high salt mobile phase (buffer B: 400 mM $NaClO_4$, 20 mM Tris–HCl, pH 6.8, and 20% v/v acetonitrile). Oligonucleotides were detected via absorbance at 260 nm. The data shown in **Figure S1** were obtained using the PA-100 column with a flow rate of 2 mL min^{-1} with the linear gradient shown in the adjacent table. The doubly-labeled mini TAR DNA elutes more rapidly than the unlabeled TAR DNA due to the loss of negative charge upon spin probe attachment. The fractions were concentrated and buffer exchanged with water using the Amicon Ultra-3k MWCO centrifugation filter. Desalted samples were lyophilized and stored at -80 °C.

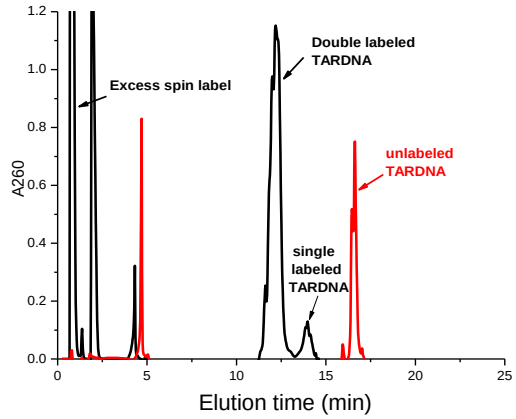

Step	Elution(min)		%Bufr B	
	start	End	Start	End
1	0	1.8	0	0
2	1.8	3.8	0	15
3	3.8	18.8	15	30
4	18.8	19.8	30	100
5	19.8	24.8	100	100
6	24.8	29.8	0	0

Fig. S1. Anion-exchange HPLC traces. The black trace is the 260-nm absorbance of a crude TAR DNA strand with two labeled phosphorothioate groups, and the red trace is the corresponding TAR DNA before labeling. The sample was doubly-labeled SLAB. The table provides the linear gradient profile.

Protocol for mini TAR DNA Analysis by Denaturing PAGE.

A nucleic acid sequencer from CBM Scientific was employed for analytical denaturing polyacrylamide gel electrophoresis (PAGE) to separate labeled and unlabeled mini TAR DNA and to monitor the extent of the reactions shown in **Fig. 2** in the main text. Analytical gels (20 cm) were made according to the manufacturer's specifications from a 25 mL solution of 20 % polyacrylamide (acrylamide: bis = 19:1) with 7 M urea in 1 X TBE (Tris-borate-EDTA) buffer, 250 μL of 10% APS (ammonium persulfate), 25 μL of N,N,N', N'-Tetramethylethylenediamine (TEMED). The running buffer was 1 X TBE. Gels were run at room temperature at 15 W and 500 V for about 2 hours. The separation of unlabeled, singly-labeled, and doubly-labeled mini TAR DNA is shown in **Figure S2**. Denaturing P. can be used on a preparative scale for separation of labeled and unlabeled mini TAR; however, the process can lead to loss of spin paramagnetism, possibly by reduction, and HPLC purification was preferred (1).

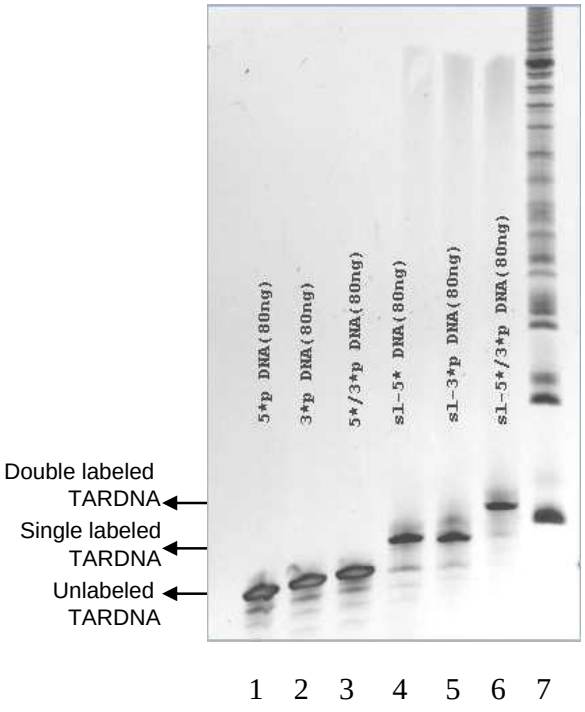

Fig. S2. This figure provides gel results showing the SLA, SLB, SLAB bands before and after spin label reaction. Lane 1: mini TAR DNA with phosphorothioate at SLA (3.0 pmoles); Lane 2: mini TAR DNA phosphorothioate at SLB (3.0 pmoles); Lane 3: mini TAR DNA phosphorothioates at SLAB (3.0 pmoles each); Lane 4: SLA after reaction; Lane 5: SLB after reaction; Lane 6: SLAB after reaction, (3.0 pmoles); Lane 7: 10 bp DNA ladder, from which the lowest band shown is from denatured 30 bp DNA.

Gel Shift Annealing Assay.

The annealing of mini TAR DNA with complementary mini TAR RNA in the presence of increasing amounts of NCp7 is the functional assay to compare the relative annealing effectiveness of doubly-labeled mini TAR DNA and unlabeled mini TAR DNA (2, 3). The gel was a 20 % polyacrylamide gel. Mixtures of mini TAR DNA, mini TAR RNA, and NCp7 were allowed to equilibrate for five minutes at room temperature in 20 mM HEPES buffer, 20 mM Na^+, 0.2 mM Mg^{2+}, pH 7.5. Gels were run at 4 ºC for 1.5 hours at 120 V. Experiments were performed at constant mini TAR DNA and mini TAR RNA concentrations of 1.4 μM. In separate lanes the TAR DNA: TAR RNA: NCp7 ratios were changed from 1:0:0 to 1:1:0 to 1:1:1 to 1:1:4.

Figures S3 a,b,c respectively contained unlabeled mini TAR DNA, doubly-labeled SLAB mini TAR DNA, and SLCD doubly-labeled mini TAR DNA. In these figures the first lane, which is mini TAR DNA stands alone and travels fastest. The second lane shows a 1:1 ratio of TAR DNA to TAR RNA, and in this lane there is evidence for the mini TAR DNA by itself, for a mini TAR RNA by itself with its band traveling slower, and for a small amount of annealed duplex, which travels slower than either of the two former bands. As respectively shown in the third and fourth lanes, the ratio of NCp7: TAR RNA: TAR DNA was then changed from 1:1:1 to 1:1:4. With increasing NCp7, the amount of annealed duplex increased for all TAR DNA constructs, both labeled and unlabeled. Compared to the lanes with unlabeled mini TAR DNA, the doubly-labeled forms of TAR DNA, showed similar annealing patterns to the unlabeled and to each other as they annealed in the presence of NCP7. The implication is that doubly-labeled constructs do not perturb the annealing function of NCp7 as it converted complementary hairpin TAR DNA and hairpin TAR RNA to a duplex.

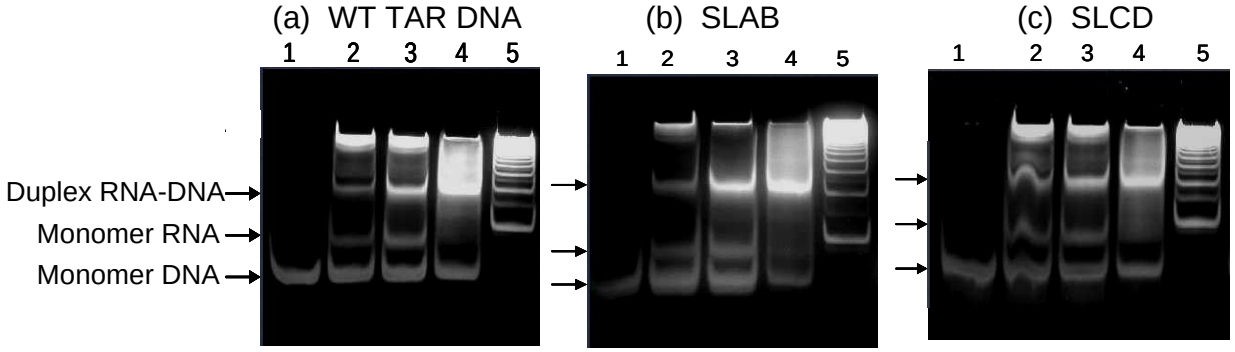

Fig. S3. This figure presents the annealing of mini TAR RNA with mini TAR DNA or with the doubly-labeled derivatives of mini TAR DNA in the presence of increasing amounts of NCp7. Non-denaturing buffer conditions were: 20 mM HEPES buffer, 20 mM Na^+, 0.2 mM Mg^{2+}, pH 7.5. Traces (**a**), (**b**), and (**c**) respectively used: (**a**) unlabeled WT mini TAR DNA; (**b**) doubly-labeled SLAB; (**c**) doubly labeled SLCD. The conditions for lanes were as follows: Lane 1, free TAR DNA; Line 2, TAR DNA: TAR RNA, 1:1 with no NCp7; Lane 3, TAR DNA: TAR RNA: NCp7, 1:1:1; Lane 4, TAR DNA: TAR RNA: NCp7, 1:1:4; Lane 5: 10 bp DNA ladder.

DEER Dipolar Evolution Transients.

Figs. S4, S5, and **S6** below provide the 17.6 GHz DEER time evolution data that were used to reconstruct the respective distance distributions in **Figs. 4, 5,** and **6** in the main text. The data in the figures below are plotted background-corrected as described in the Methods and Materials section of the main text. All data were normalized to represent the DEER signal, which is unity at zero time, and distributed vertically for clarity.

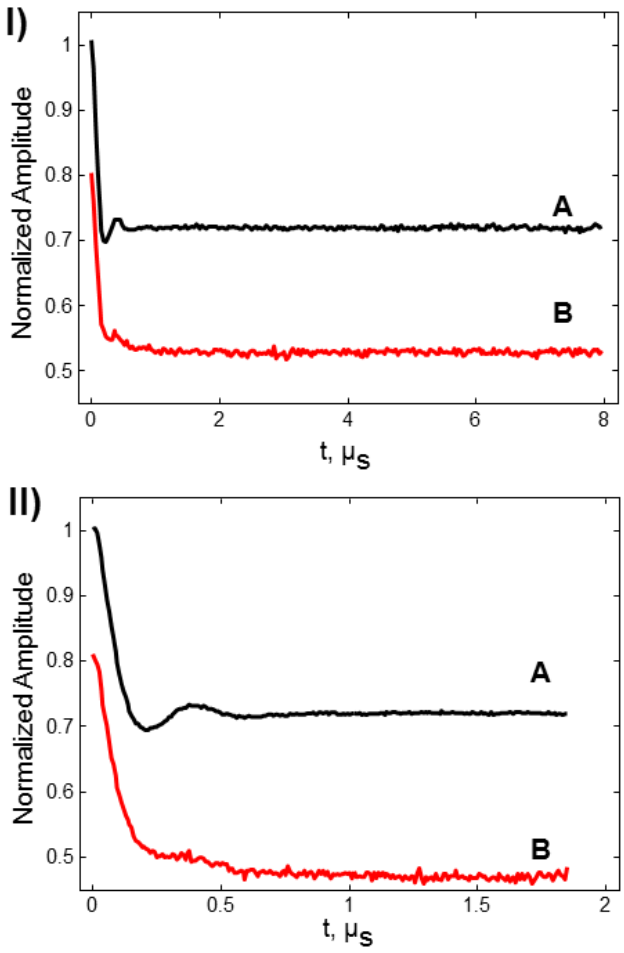

Fig. S4. These are the time evolution data corresponding to the DEER distributions in **Fig. 4A and 4B** in the Results Section. Here, the transients labeled **A** are for SLCD by itself and correspond to the DEER distribution of **Fig. 4A**. The transients labeled **B** are for SLCD with the addition of 4 equivalents of NCP7 and correspond to the DEER distribution of **Fig. 4B**. The transients are shown over both a longer time view (Panel I) of ~8 μs, which provided information on the presence of inter-label distances greater than 60 Å, and over a shorter time view (Panel II) of ~2 μs, which was used to reconstruct the inter-label distribution below 60 Å. Distance distributions were generated from short-term data; long term data served to verify the absence of very long distances. Data averaging times for Panel (**I**) were 54 min (A), 15 h (B) and for Panel (**II**) both (A) and (B) were 30 min. All data were taken at 65 ºK.

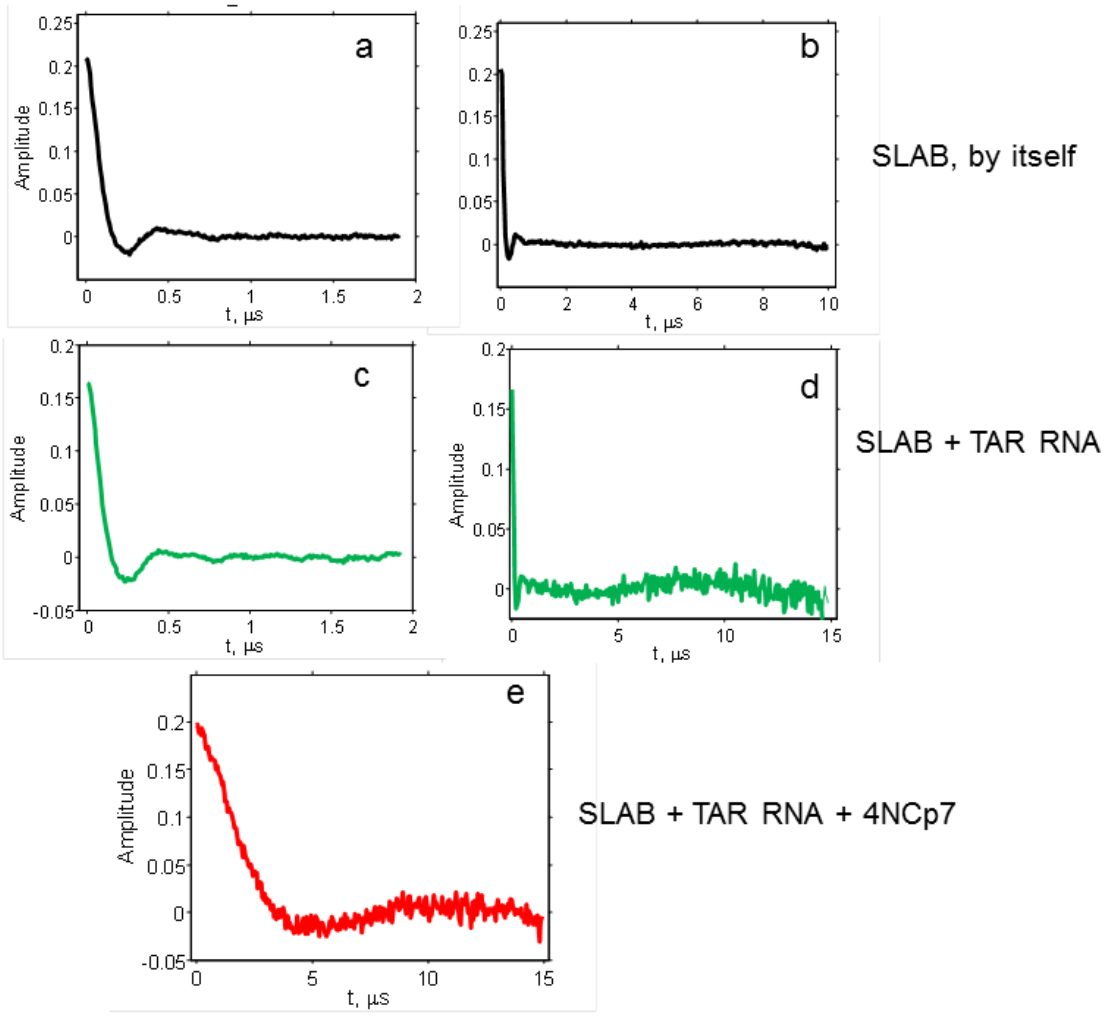

Fig. S5. These are the time evolution data corresponding to the DEER distributions in **Fig. 5** in the Results Section for: SLAB DNA by itself, SLAB DNA+ TAR RNA with no NCp7, and SLAB DNA + TAR RNA + 4X NCp7. The time domain data recorded over approximately 2 µs were sufficient to reconstruct the inter-label distributions, P(r), below 60 Å for SLAB DNA by itself and SLAB DNA+ TAR RNA with no NCp7. The time-domain data of the dipolar evolution, recorded over 15 µs, were sufficient to reconstruct the distance of ~7.5 nm for the duplex RNA-DNA arising from SLAB DNA + TAR RNA + 4X NCp7. Deuterated solutions and low ionic strength were used in all three cases. Data averaging time were as follows: Panel (**a)**, 30 min; Panel (**b)**, 3 h; Panel (**c)**, 30 min; Panel (**d)**, 14 hr; Panel (**e)**, 11.5 hr. All data were taken at 65 ºK.

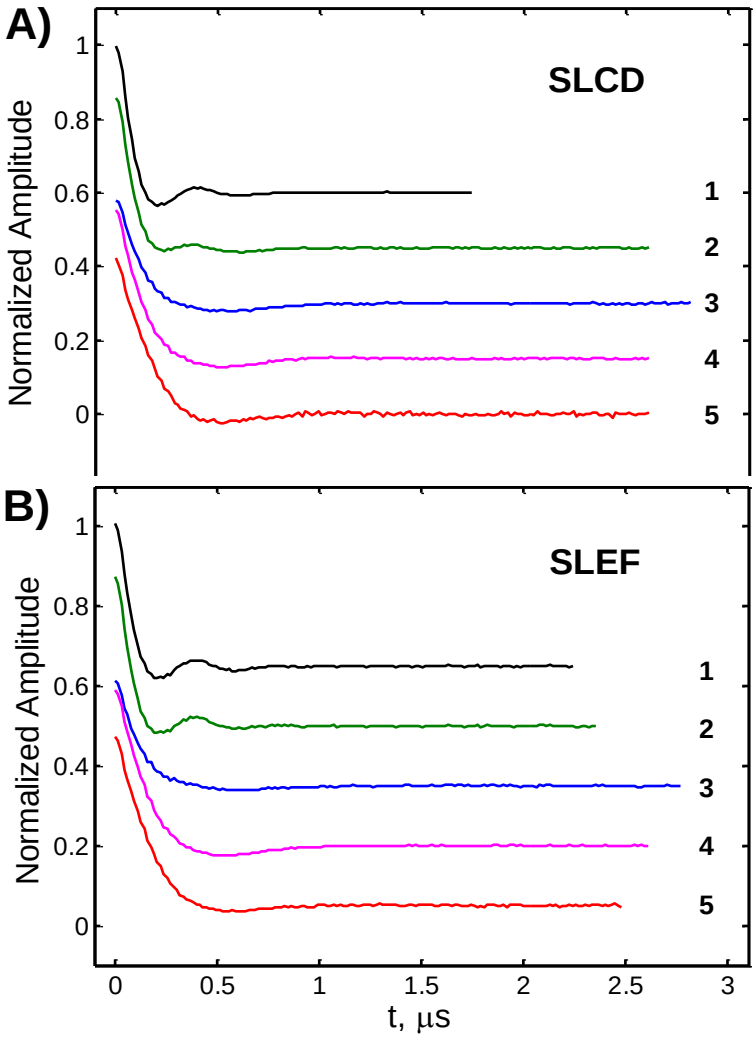

Fig. S6. These are the time evolution data corresponding to the DEER distributions, P(r), shown in **Figs. 6 a** and **6 b** of the main text and in **Figs. S8** and **S9**. The data in the figure are plotted background-corrected as described in the Materials and Methods section of the main text. Panel (A) corresponds to SLCD. Here, individual curves use color-coding of the respective panels in the main text and additionally are numbered as: (1) black, SLCD by itself; (2) green, a 1:1 mixture of SLCD + mini TAR RNA; (3) blue, a thermally-annealed mixture of 1:1 mixture of doubly-labeled SLCD and mini TAR RNA; (4) magenta, a 1:1:1 mixture of SLCD mini TAR DNA to mini TAR RNA to NCp7; (5) red, a 1:1:4 mixture of SLCD mini TAR DNA to mini TAR RNA to NCp7. Panel (B) is for SLEF and has the same time-scale, color-coding, and data numbering as Panel (**A**). Data averaging time for SLCD was 10 min for data set (1) and 43 min for the rest. For SLEF these were 10 min for (1), 21 min for (2) and (5), and 43 min for (3) and (4). All data were taken at 65 K.

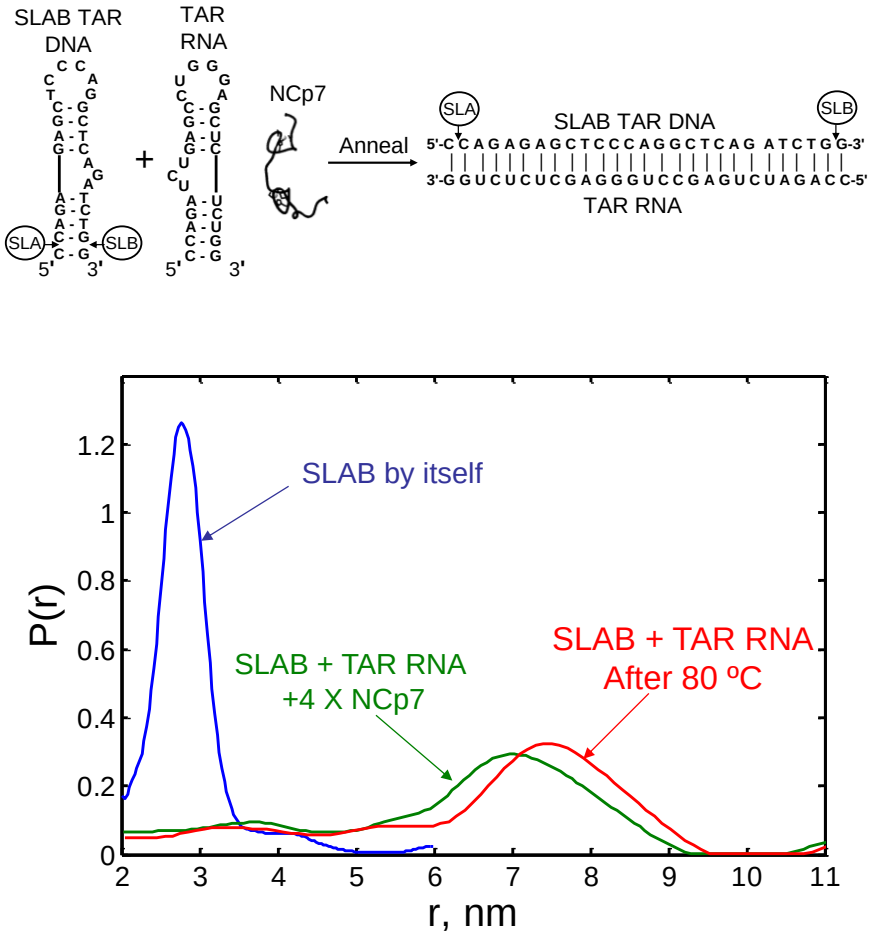

Fig. S7. A comparison of the inter label distance distribution taken in protonated solvent between doubly-labeled SLAB mini TAR DNA by itself (blue trace), doubly-labeled SLAB mini TAR DNA annealed in the presence of a 1:1:4 of SLAB mini TAR DNA to unlabeled mini TAR RNA: to NCp7 (green trace) , and doubly-labeled SLAB mini TAR DNA thermally annealed at 80 ºC with mini TAR RNA (red trace). Sample conditions: 20 mM HEPES, 20 mM NaCl, 0.2 mM $MgCl_2$, pH 7.5. Samples were frozen in 10 % glycerol to prevent tube breakage. These were early samples prepared in protonated solvent, and the position of the peaks at long distances (> 60 Å) is only accurate to within 5 Å. The purpose of the figure is to show the similarity of the NCp7-annealed and the thermally annealed 1:1 mixtures of TAR DNA and TAR RNA.

Calculated Inter-NO Distances – Comparison of DEER Experimental Results and NASNOX Predictions

Using NASNOX, an average inter-label NO distance $\langle r_{NASNOX} \rangle$ was calculated from the ensemble of allowed rotamers, and the RMS uncertainty σ_{NASNOX} in the distance between NO groups determined. For a Gaussian distribution of inter-nitroxide distances, this latter uncertainty σ translates readily into the full-width at half height, $W_{1/2}$, of the double-label distance distribution, where $W_{1/2} = (2)^{3/2} (0.693)^{1/2} \sigma$. Predicted distances and widths of the inter-nitroxide distance distribution were then compared to corresponding experimental DEER results $\langle r_{DEER} \rangle$ and σ_{DEER}. Additionally, histograms of the double-label inter-nitroxide distance distribution were computed from NASNOX ensembles (4, 5) for comparison to the experimentally determined distributions obtained by PDS. An overlay of PDS results for SLCD (**Fig. 6a**) and SLEF (**Fig. 6b**) and the corresponding histograms of the expected distance distributions for the double labels are provided in the **Supporting Material, Figs. S8** and **S9**. The histograms shown in **Figs. S8** and **S9** were obtained both for the double labels residing in the unperturbed mini TAR DNA upper stem-loop and for the double labels of SLCD and SLEF residing in the DNA-RNA duplexes.

In **Table S1** the experimentally measured distances between diametrically opposite nitroxide doubly-labeled sites in SLAB, SLCD, and SLEF doubly-labeled forms of mini TAR DNA were all found within 1 Å of $\langle r_{DEER} \rangle$ = 27 Å with inter-nitroxide distribution widths which diminished in the order SLAB, SLCD, SLEF. Using a dodecamer B-form DNA duplex (PDB 1CS2 (6, 7)) and NASNOX, the NO groups of eleven separate, diametrically opposite spin labels provided estimates of $\langle r_{NASNOX} \rangle$ = 26.0 Å and σ_{NASNOX} = 1.9 Å, both in good agreement with our experiments on diametrically opposite labels in duplex regions of mini TAR DNA. Since the inter-phosphorous distance between diametrically opposed phosphates is 17.7 Å (7) and the average inter-nitroxide distance of diametrically opposite nitroxides per **Table S1** was 26.9 Å, then the additional radial distance of a spin label NO group from its attaching phosphorothioate would be about 4.6 Å [= (26.9 – 17.7)/2].

Using a 13-mer DNA-RNA duplex model (PDB 1EFS (8), application of NASNOX with spin labels attached *in silico* provided from DNA-RNA duplexes estimates of the expected values of $\langle r_{NASNOX} \rangle$ and σ_{NASNOX}. Between spin labels attached 10 bases apart in the DNA strand of the RNA-DNA duplex it was found that $\langle r_{NASNOX} \rangle$ = 36.5 Å and σ_{NASNOX} = 4.7 Å (8), to be compared with $\langle r_{DEER} \rangle$ = 34.8 Å and σ_{DEER} = 5.9 Å from SLEF in the mini TAR DNA-RNA complex. Between spin labels attached 8 bases apart to the DNA strand of the RNA-DNA duplex it was found that $\langle r_{NASNOX} \rangle$ = 36.3 Å and σ_{NASNOX} = 4.6 Å, to be compared with $\langle r_{DEER} \rangle$ = 35.1 Å and σ_{DEER} = 4.6 Å from SLCD in the mini TAR DNA-RNA complex. In both cases the agreement between experiment and prediction was good. The similarity of inter-NO distances of SLCD, 8 bases apart, and SLEF, 10 bases apart, follows because the distance change along the direction of the helix is offset by the distance change due to helical rotation of nitroxide side chains perpendicular to the helical axis.

To approximate the distance on the mini TAR DNA strand between phosphorothioate-attached spin labels near the opposite ends of the 27-mer duplex as SLA and SLB would be after they are incorporated in a TAR DNA-RNA duplex, we have estimated distances from the axial rise per residue and the angular rotation per residue about the helix axis (9, 10). The rise based on the

average of four different RNA-DNA duplexes, is 2.90 ± 0.08 Å/base, and the rotation per residue is 32 ± 1º (9). Per our own work on diametrically opposite bi-labels, the distance of the label nitroxide from the helix axis is 13.5 Å. For a 25 phosphate separation, these numbers (rise per base, rotation per residue, and distance of nitroxide from helix axis) predict a distance between labels of $\langle r \rangle$ = 74.5 ± 2.8 Å. This simple geometric approach assumes a straight helix. The literature indicates that there can be some local mixture and flexibility variation between A-type and B-type helical forms within the mixed RNA-DNA helix (9); such mixture and flexibility may contribute to the 19.5 Å breadth of the SLA-SLB distance distribution in the RNA-DNA duplex. Given the approximate way of estimating the long SLA-SLB inter-nitroxide distance, the agreement between prediction and DEER results is good.

Table S1.
Inter-label Distances and Peak Widths of Doubly-Labeled mini TAR DNA

Experimental DEER Inter-label Distances and Widths				**Computed Estimates, Inter-label Distances and Widths**
Sample	**$\langle r_{DEER} \rangle$ (Å)**[a]	**$W_{1/2}$ (Å)**[a]	**σ_{DEER} (Å)**[a]	
SLAB by itself	27.5 ± 0.5	7.0 ± 0.5	3.0 ± 0.2	$\langle r_{NASNOX} \rangle$ = 26.0 Å σ_{NASNOX} = 1.9 Å (b)
SLCD by itself	26.8 ± 0.4	5.2 ± 0.4	2.2 ± 0.2	
SLEF by itself	26.3 ± 0.4	4.3 ± 0.4	1.8 ± 0.2	
1:1:4 SLCD/mini TAR RNA/NCp7	35.1 ± 0.6	10.8 ± 1.0	4.6 ± 0.4	$\langle r_{NASNOX} \rangle$ = 36.3 Å σ_{NASNOX} = 4.6 Å (c)
1:1:4 SLEF/mini TAR RNA/NCp7	34.8 ± 0.6	14.0 ± 1.0	5.9 ± 0.4	$\langle r_{NASNOX} \rangle$ = 36.5 Å σ_{NASNOX} = 4.7 Å (d)
1:1:4 SLAB/mini TAR RNA/NCp7	76.5 ± 2.0	19.5 ± 2.0	8.3 ± 0.8	$\langle r \rangle$ = 74.5 ± 2.8 Å (e)

[a] $\langle r_{DEER} \rangle$ and $W_{1/2}$ are the respective experimental inter-label distance and the full peak width at half height as determined experimentally by DEER. σ_{DEER} is the RMSD of the DEER peak, and assuming a Gaussian shape, $W_{1/2} = (2)^{3/2} (0.693)^{1/2} \sigma_{DEER}$.

[b] By use of the dodecamer DNA duplex (PDB 1CS2) (6, 7) and NASNOX algorithm, the NO groups of eleven separate, diametrically opposite spin labels provided this estimate of $\langle r_{NASNOX} \rangle$ and σ_{NASNOX} .

[c] By use of a 13-mer DNA-RNA duplex (PDB 1EFS) (8) and the NASNOX algorithm, doubly-labeled DNA sites 8 bases apart, like SLC and SLD, were predicted to have these values for $\langle r_{NASNOX} \rangle$ and σ_{NASNOX} .

[d] By use of a 13-mer DNA-RNA duplex (PDB 1EFS) (8) and the NASNOX method, double-labeled DNA sites 10 bases apart, like SLE and SLF, were predicted to have these values for $\langle r_{NASNOX} \rangle$ and σ_{NASNOX} .

[e] Based on an axial rise of 2.90 ± 0.08 Å/base, a helical rotation per residue of 32 ± 1º (9) a separation between labeling sites of 25 phosphates, and a radial distance of the label nitroxide from the helix axis of 13.5 Å (per **Table S1** above) , this distance $\langle r \rangle$ was geometrically predicted.

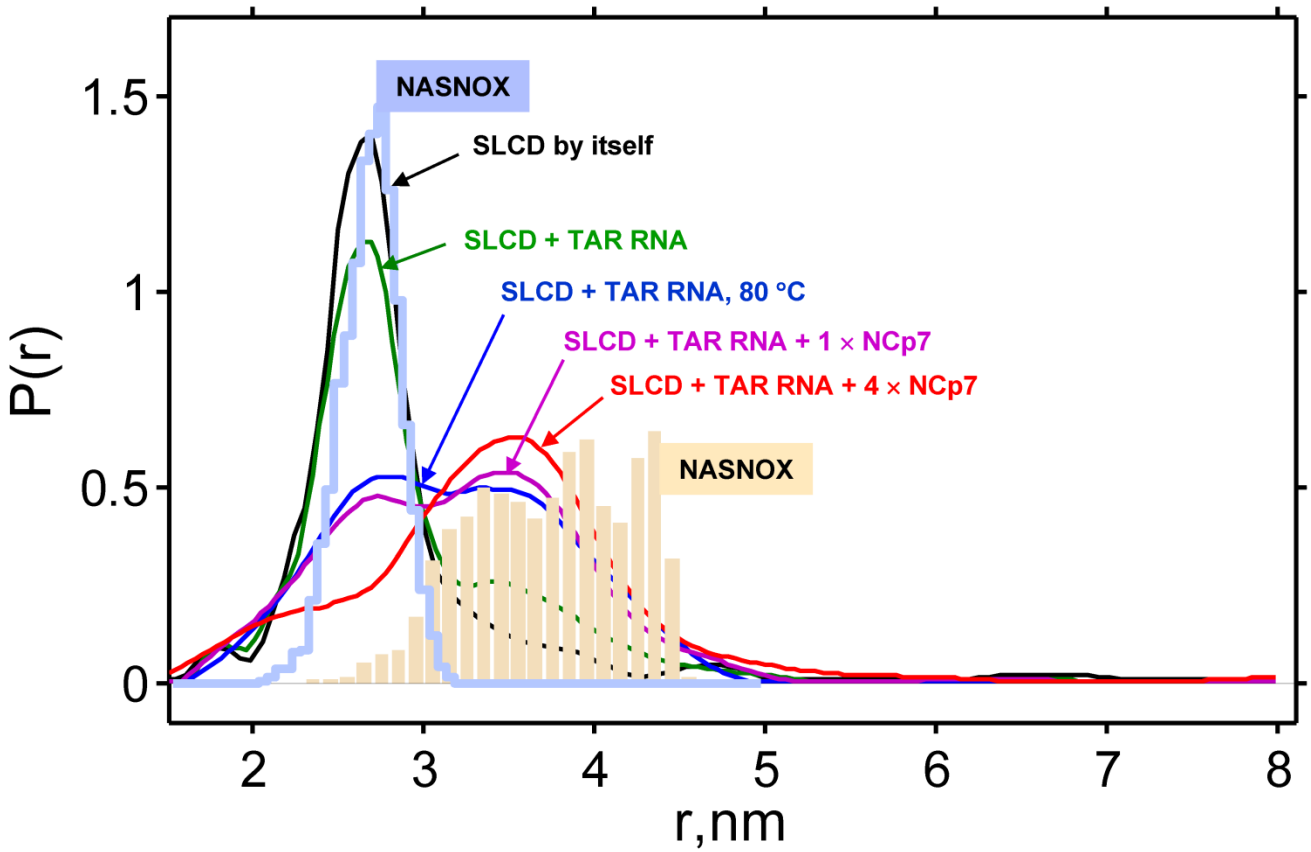

Fig. S8. The inter-nitroxide distance distribution from SLCD shown in **Fig. 6a** in the main text compared to the histograms of the distance distributions computed by NASNOX for the following: 1) The histogram (light blue) for a diametrically opposite pair of phosphorothioate-attached spin labels located on a duplex DNA strand specifically from PDB structure 1CS2, bases 6 & 20 from ref. (6)). 2) The histogram (beige) for a pair of phosphorothioate-attached spin labels 8 bases apart on the DNA strand of a DNA-RNA duplex (specifically from the PDB structure 1EFS, bases 3 & 11 from ref. (8).

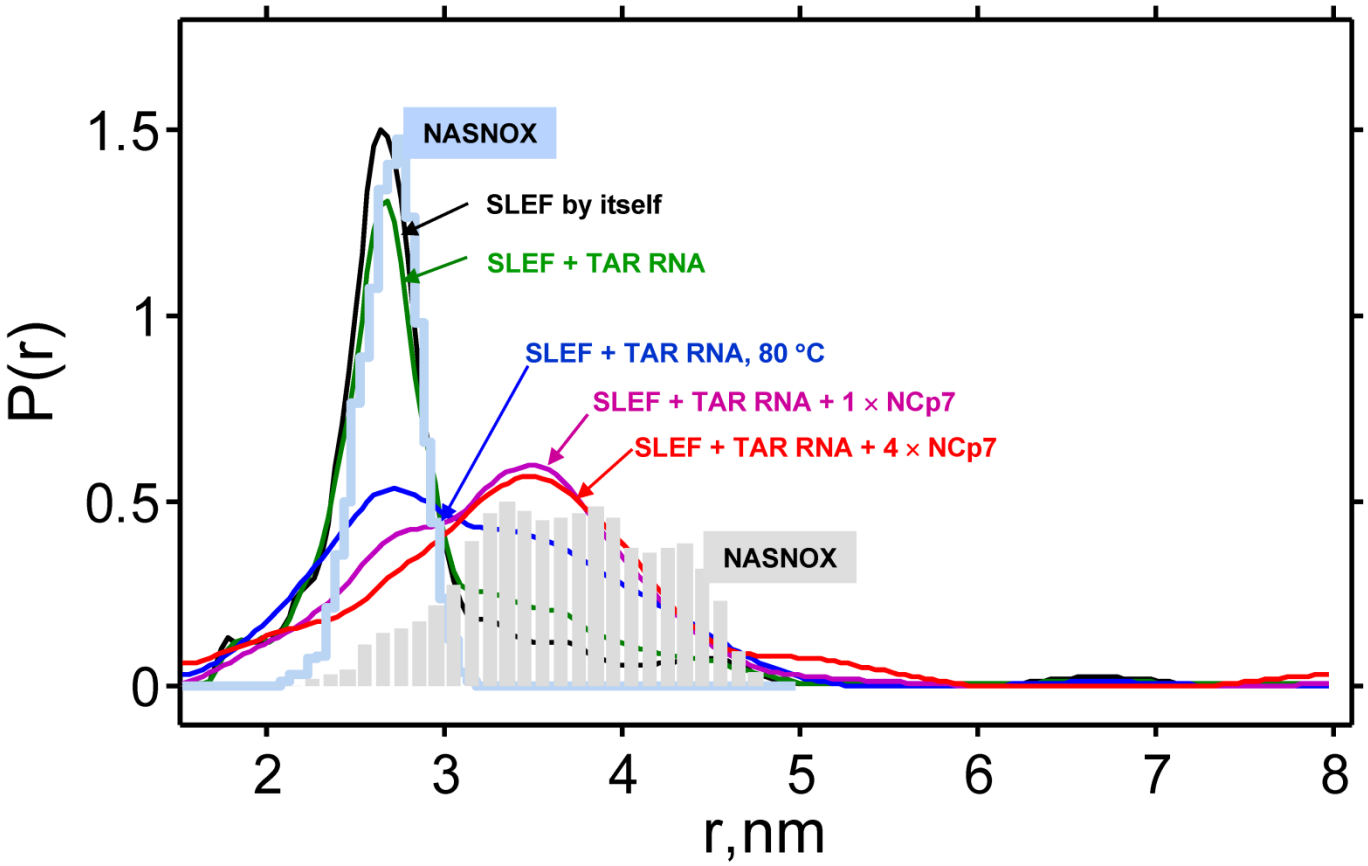

Fig. S9. A comparison of the inter-nitroxide distance distribution from SLEF shown in **Fig. 6b** in the main text to the histograms of the distance distributions computed by NASNOX for the following: 1) The histogram (light blue) for a diametrically opposite pair of phosphorothioate-attached spin labels located on a duplex DNA strand (specifically from PDB structure 1CS2, bases 6 & 20 from ref. (6)). 2) The histogram (grey) for a pair of phosphorothioate-attached spin labels 10 bases apart on the DNA strand of a DNA-RNA duplex (specifically from the PDB structure 1EFS, bases 2 & 12 from ref. (8).

PDS Versus Fluorescence Resonance Energy Transfer (FRET) in Application to TAR.

The technique of FRET at different levels of sophistication has been used to follow inter-probe distance change, conformational bending, and annealing of TAR DNA and TAR RNA in the presence of NCp7 (11-18). Solution FRET initially provided qualitative information about RNA unwinding and annealing in the presence of NCp7 (12, 13). Time-resolved FRET decay has provided evidence for different species with several different decay times, and by inference, evidence for several different conformations of frayed, destabilized TAR DNA (19, 20). FRET correlation spectroscopy showed evidence for the kinetic interconversion of destabilized stem loops (21, 22). More elegant single molecule FRET, requiring resolution of individual, immobilized, fluorescently labeled biomolecules has provided histograms of single molecule FRET efficiencies. The evidence from these histograms, which were taken under ambient temperature conditions, is that interconverting conformers of duplex and stem-loop structures were brought about by NCp7 (11, 14-18). Such distributions may well translate into conformers with different inter-label distances, but it is noteworthy that FRET histograms are appropriately shown as a function of FRET efficiency not of inter-probe distance (11). The Förster mechanism for FRET has in principle an r^{-6} inter-fluorophore distance dependence but with somewhat uncertain factors as discussed by Gopich and Szabo (23). Also, FRET requires a larger probe size and longer tethers than nitroxide probes, as well as the need of multiple FRET pairs of different Förster radii to cover a distance range of, e.g., 1-10 nm. The probe orientation factor for FRET often needs to be determined independently. The r^{-3} inter-nitroxide distance dependence of PDS means that PDS will more directly yield structural information over the 1-9 nm range, including distance distributions and multiple conformers. The aggregating properties of 1-55 NCp7, which are essential to its annealing behavior, are an impediment to the fluorescence process because of the light scattering of aggregates. In brief, PDS and FRET complement each other for study of oligonucleotide structures; PDS gives more detailed distance information, and FRET is at present more amenable to ambient temperature measurements.

REFERENCES

1. Sun, Y., Z. Zhang, V. M. Grigoryants, W. K. Myers, F. Liu, K. A. Earle, J. H. Freed, and C. P. Scholes. 2012. The Internal Dynamics of Mini c TAR DNA Probed by Electron Paramagnetic Resonance of Nitroxide Spin-Labels at the Lower Stem, the Loop, and the Bulge. Biochemistry 51:8530–8541.
2. Vo, M. N., G. Barany, I. Rouzina, and K. Musier-Forsyth. 2006. Mechanistic studies of mini-TAR RNA/DNA annealing in the absence and presence of HIV-1 nucleocapsid protein. J Mol Biol 363:244-261.
3. Vo, M. N., G. Barany, I. Rouzina, and K. Musier-Forsyth. 2009. HIV-1 nucleocapsid protein switches the pathway of transactivation response element RNA/DNA annealing from loop-loop "kissing" to "zipper". J Mol Biol 386:789-801.
4. Price, E. A., B. T. Sutch, Q. Cai, P. Z. Qin, and I. S. Haworth. 2007. Computation of nitroxide-nitroxide distances in spin-labeled DNA duplexes. Biopolymers 87:40-50.
5. Qin, P. Z., I. S. Haworth, Q. Cai, A. K. Kusnetzow, G. P. Grant, E. A. Price, G. Z. Sowa, A. Popova, B. Herreros, and H. He. 2007. Measuring nanometer distances in nucleic acids using a sequence-independent nitroxide probe. Nat Protoc 2:2354-2365.
6. Leporc, S., O. Mauffret, G. Tevanian, E. Lescot, M. Monnot, and S. Fermandjian. 1999. An NMR and molecular modelling analysis of d(CTACTGCTTTAG). d(CTAAAGCAGTAG) reveals that the particular behaviour of TpA steps is related to edge-to-edge contacts of their base-pairs in the major groove. Nucleic Acids Res 27:4759-4767.
7. Cai, Q., A. K. Kusnetzow, W. L. Hubbell, I. S. Haworth, G. P. Gacho, N. Van Eps, K. Hideg, E. J. Chambers, and P. Z. Qin. 2006. Site-directed spin labeling measurements of nanometer distances in nucleic acids using a sequence-independent nitroxide probe. Nucleic Acids Res 34:4722-4730.
8. Hantz, E., V. Larue, P. Ladam, L. Le Moyec, C. Gouyette, and T. Huynh Dinh. 2001. Solution conformation of an RNA--DNA hybrid duplex containing a pyrimidine RNA strand and a purine DNA strand. Int J Biol Macromol 28:273-284.
9. Gyi, J. I., A. N. Lane, G. L. Conn, and T. Brown. 1998. Solution structures of DNA.RNA hybrids with purine-rich and pyrimidine-rich strands: comparison with the homologous DNA and RNA duplexes. Biochemistry 37:73-80.
10. Saenger, W. 1984. Principles of Nucleic Acid Structure. Springer-Verlag, New York.
11. Wang, H., K. Musier-Forsyth, C. Falk, and P. F. Barbara. 2013. Single-molecule spectroscopic study of dynamic nanoscale DNA bending behavior of HIV-1 nucleocapsid protein. The journal of physical chemistry. B 117:4183-4196.
12. Chan, B., K. Weidemaier, W. T. Yip, P. F. Barbara, and K. Musier-Forsyth. 1999. Intra-tRNA distance measurements for nucleocapsid proteindependent tRNA unwinding during priming of HIV reverse transcription. Proc Natl Acad Sci U S A 96:459-464.
13. Hong, M. K., E. J. Harbron, D. B. O'Connor, J. Guo, P. F. Barbara, J. G. Levin, and K. Musier-Forsyth. 2003. Nucleic acid conformational changes essential for HIV-1 nucleocapsid protein-mediated inhibition of self-priming in minus-strand transfer. J Mol Biol 325:1-10.
14. Cosa, G., E. J. Harbron, Y. Zeng, H. W. Liu, D. B. O'Connor, C. Eta-Hosokawa, K. Musier-Forsyth, and P. F. Barbara. 2004. Secondary structure and secondary structure dynamics of DNA hairpins complexed with HIV-1 NC protein. Biophys J 87:2759-2767.

15. Liu, H. W., G. Cosa, C. F. Landes, Y. Zeng, B. J. Kovaleski, D. G. Mullen, G. Barany, K. Musier-Forsyth, and P. F. Barbara. 2005. Single-molecule FRET studies of important intermediates in the nucleocapsid-protein-chaperoned minus-strand transfer step in HIV-1 reverse transcription. Biophys J 89:3470-3479.
16. Liu, H. W., Y. Zeng, C. F. Landes, Y. J. Kim, Y. Zhu, X. Ma, M. N. Vo, K. Musier-Forsyth, and P. F. Barbara. 2007. Insights on the role of nucleic acid/protein interactions in chaperoned nucleic acid rearrangements of HIV-1 reverse transcription. Proc Natl Acad Sci U S A 104:5261-5267.
17. Zeng, Y., H. W. Liu, C. F. Landes, Y. J. Kim, X. Ma, Y. Zhu, K. Musier-Forsyth, and P. F. Barbara. 2007. Probing nucleation, reverse annealing, and chaperone function along the reaction path of HIV-1 single-strand transfer. Proc Natl Acad Sci U S A 104:12651-12656.
18. Wang, H., Y. S. Yeh, and P. F. Barbara. 2009. HIV-1 nucleocapsid protein bends double-stranded nucleic acids. J Am Chem Soc 131:15534-15543.
19. Beltz, H., E. Piemont, E. Schaub, D. Ficheux, B. Roques, J. L. Darlix, and Y. Mély. 2004. Role of the structure of the top half of HIV-1 cTAR DNA on the nucleic acid destabilizing activity of the nucleocapsid protein NCp7. J Mol Biol 338:711-723.
20. Bernacchi, S., S. Stoylov, E. Piemont, D. Ficheux, B. P. Roques, J. L. Darlix, and Y. Mély. 2002. HIV-1 nucleocapsid protein activates transient melting of least stable parts of the secondary structure of TAR and its complementary sequence. J Mol Biol 317:385-399.
21. Beltz, H., J. Azoulay, S. Bernacchi, J. P. Clamme, D. Ficheux, B. Roques, J. L. Darlix, and Y. Mély. 2003. Impact of the terminal bulges of HIV-1 cTAR DNA on its stability and the destabilizing activity of the nucleocapsid protein NCp7. J Mol Biol 328:95-108.
22. Godet, J., and Y. Mély. 2010. Biophysical studies of the nucleic acid chaperone properties of the HIV-1 nucleocapsid protein. RNA Biol 7:687-699.
23. Gopich, I. V., and A. Szabo. 2011. Theory of Single-Molecule FRET Efficiency Histograms. In Single-Molecule Biophysics. John Wiley & Sons, Inc. 245-297.